Biomedicine & Pharmacotherapy 133 (2021) 111050

Contents lists available at ScienceDirect

Biomedicine & Pharmacotherapy

journal homepage: www.elsevier.com/locate/biopha

Original article

Design, synthesis and biological evaluation of novel pyxinol derivatives with anti-heart failure activity

Junli Liu [a], Yunhe Liu [a], Hui Yu [a], Ying Zhang [a,b], Alan Chen-Yu Hsu [d], Mingming Zhang [c], Yawei Gou [c], Wei Sun [c], Fang Wang [c], Pingya Li [a], Jinping Liu [a,*]

[a] School of Pharmaceutical Sciences, Jilin University, Fujin Road 1266, Changchun 130021, China
[b] The First Hospital of Jilin University, Changchun 130021, China
[c] College of Basic Medical Sciences, Jilin University, Changchun 130021, China
[d] Priority Research Centre for Healthy Lungs, Faculty of Health and Medicine, The University of Newcastle, Newcastle, NSW 2305, Australia

ARTICLE INFO

Keywords:
Pyxinol
Fatty acid esters
ACE inhibition
Molecular docking
Heart failure
Metabolomics

ABSTRACT

Heart failure (HF) is an important and leading cause of substantial morbidity and mortality globally. The angiotensin-converting enzymatic (ACE) is the causative source for congestive heart failure. Natural products and its derivatives play a vital role in drug discovery and development owing to their efficacy and low toxicity. Pyxinol is a potent natural agent for cardiovascular disease. Thus we investigated the effect on ACE and HF of pyxinol derivatives. We designed and synthesized 32 novel fatty acid ester derivatives of pyxinol *via* esterification. Among them, compounds **2e** (IC_{50}=105 nM) and **3b** (IC_{50}=114 nM) displayed excellent ACE inhibitory activity *in vitro*, and exhibited non-toxic to H9c2 cells. The interactions between ACE and compounds were predicted by molecular docking respectively. In verapamil-induced zebrafish HF model, the activity assay showed that these two derivatives could improve cardiovascular physiological indexes including heart beats, venous congestion, heart dilation, cardiac output, ejection fraction and fractional shortening in a dose-dependent manner. A UPLC-QTOF-MS-based serum metabolomics approach was applied to explore the latent mechanism. A total of 25 differentiated metabolites and 8 perturbed metabolic pathways were identified. These results indicated that pyxinol fatty acid ester derivatives **2e** and **3b** might be considered as potent drug candidates against heart failure and deserved further research and development.

1. Introduction

Heart failure (HF), sometimes known as congestive HF, is a complex clinical disease that results from contractile and/or diastolic functional impairment of the heart [1,2]. HF is an important and leading cause of substantial morbidity and mortality globally [3,4]. Angiotensin-converting enzyme (ACE), an important enzyme in renin angiotensin aldosterone system that catalyzes the conversion of inactive angiotensin I to the potent angiotensin II [5], regulates blood pressure, blood volume and body fluid balance [6], and plays a considerable role in HF [7]. Research in effective drugs with ACE inhibition and anti-HF activity are therefore urgently required.

Natural products play a vital role in drug discovery and development owing to their efficacy and low toxicity [8]. Pyxinol, (20*S*,24*R*)-epoxy-dammarane-3β, 12β, 25-triol, was isolated firstly from a lichen *Pyxine endochrysina* N_{YL} in 1972 [9], and then was isolated from the Fern *Notholaena rigidain* in 1996 [10]. Later, it was also reported to be isolated from *Betula humilis* [11] and *Salvia barrelieri* [12], respectively. Interestingly, pyxinol is one of the main metabolites of protopanaxadiol (an aglycon of ginsenosides) in humans and rats [13,14]. Our group had prepared this natural product with high yield by treating protopanaxadiol with 3-chloroperoxy-benzoic acid [15]. Pyxinol exhibited multiple pharmacological activities such as inhibitions of myocardial ischemic injury [16,17], the occurrence and development of cisplatin-induced kidney injury [18], hyperglycemia [19], neurodegenerative disease [20], cerebral ischemia [15], malarial infection [21], cancer [22], depression [23] and inflammatory diseases [24].

Meanwhile, continuous efforts have been made to structurally modify pyxinol with the hope of improving biological activities. The relevant reported included amide derivatives or 3-hydroxyaminated derivatives with anti-multidrug resistance activity [25,26], aliphatic amino derivatives or nitrated derivatives with antibacterial activity [27,

* Corresponding author.
E-mail address: liujp@jlu.edu.cn (J. Liu).

https://doi.org/10.1016/j.biopha.2020.111050
Received 21 September 2020; Received in revised form 15 November 2020; Accepted 19 November 2020
Available online 30 November 2020

28], nitrogen-containing esterified derivatives or oxime derivatives with anti-inflammatory activity [29,30], and furoxan derivatives with enhancing NO releasing capacity [31]. However, the research on the pyxinol derivatives with ACE inhibition and anti-heart failure effect is quite limited. Among the structural modification, esterification of pyxinol with fatty acids was important in enhancing efficacy [32,33]. It was also reported that the fatty acid esters of ginsenosides might be the real effective ingredients *in vivo* [34,35].

Zebrafish and its embryo are characterized by small, transparent and enabling nonintrusive, high resolution visualization of developmental stages during organogenesis *in vivo* [36]. Because the structures, functions electrical and mechanical properties of Zebrafish's heart are highly comparable with mammalian heart, Zebrafish could respond very similarly to drug treatment as humans [37–39]. Untargeted metabolomics, a systematic method to profile diverse classes of metabolites in biological samples, was prospective for understanding the underlying biochemical mechanism and giving insight into the physiological and functional states of the investigated zebrafish [40–42].

In this study, we designed and synthesized 32 fatty acid ester derivatives by the acylation of pyxinol with saturated fatty acids (C2-C8) introduced to 3-, 12- and 25-positions with good yields. These products were then assessed for their effects on ACE *in vitro* and HF in zebrafish (*Danio rerio*). The interactions between ACE and the active compounds were predicted by molecular docking. Furthermore, the serum metabolomics analysis was performed to discuss the potential mechanism.

2. Results and discussion

2.1. Compounds design

Generally speaking, the esterified derivatives could increase the lipophilic solubility and permeability, which would increase their transmembrane absorption [43]. Owing to their structural diversity, the conjugation of fatty acid to specific pharmacological agents has been shown to enhance candidate compound potency in certain contexts [44–48]. Pharmacokinetic studies also demonstrated that the fatty acid (especially fatty chains $\leq$ 8 carbons) esterification derivatives of ginsenoside might be the real active ingredients and could sustain longer in the body [34,47,49].

Specially, in this study, the target-based drug design was used to synthesize the pyxinol derivatives. ACE active sites were divided into three pockets (S1, S2 and S1'). S1 site included Ala354, Glu384, Tyr523 and Ser355 residues, S2 site included Gln281, His353, Lys511, His513, Tyr520 and Arg522 residues, while S1' site only included Glu162 residue [50–52]. Furthermore, the zinc ion also plays an important role at the ACE active site [53], it is partly responsible for the binding strength between ACE and their inhibitors [54]. Pyxinol, the lead compound, only interacts with Tyr523 (2.8 Å) in ACE (PDB ID: 1O8A) S1 subsite with a binding energy (ΔG) of -8.57 kcal/mol (Fig. 1A). In order to increase the interaction between compounds and target, the ester group was introduced to form more hydrogen bonds with His513 (2.0 Å), Tyr523 (2.0 Å) and His353 (1.8 Å) in S1 and S2 subsites with a binding energy (ΔG) of -10.14 kcal/mol (Fig. 1B). The docking result showed that esterified derivatives might promote the biological activity of pyxinol by increase the interaction effect.

According to previous literatures, the structural modification at C-3, C-12, or C-25 hydroxy such as amide derivatives or 3-hydroxyaminated derivatives [25,26], aliphatic amino derivatives or nitrated derivatives [27,28], nitrogen-containing esterified derivatives or oxime derivatives [29,30], and furoxan derivatives [31] could all significantly improve the biological activity of pyxinol with low toxicity. Accordingly, we anticipated that fatty acid conjugated pyxinol might result in new leads possessing good pharmacological activities. The saturated fatty acids (C2-C8) were chosen to modify the C-3, C-12, or C-25 of pyxinol in present study (Fig. 2).

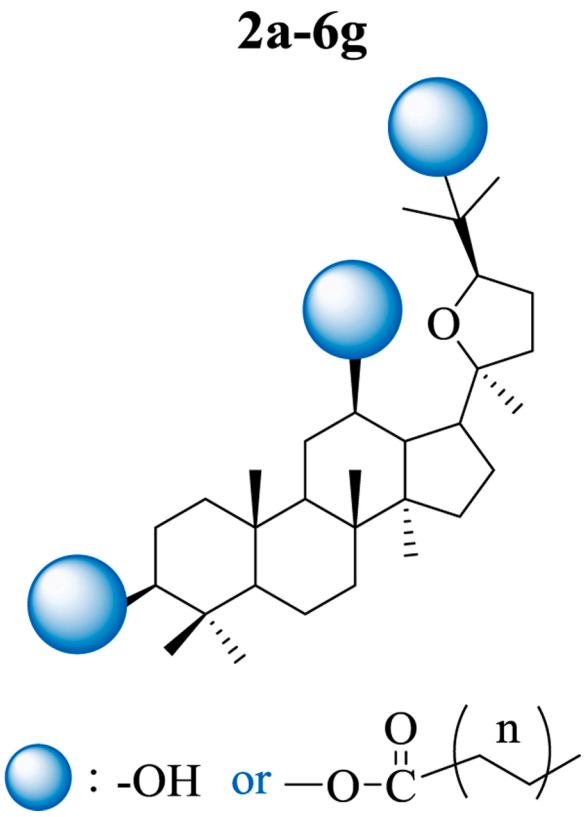

Fig. 2. Design of fatty acid derivatives of pyxinol.

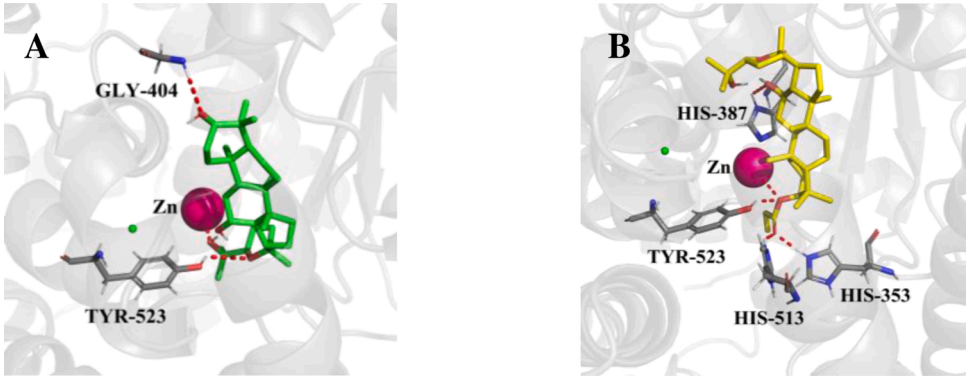

Fig. 1. A) Best predicted binding mode of pyxinol at ACE binding site. B) Best predicted binding mode of **2b** at ACE binding site.

2.2. Chemistry

The derivatives **2b-2f** and **3a-4e** were synthesized through *O*-acylation from pyxinol (**1**) using corresponding acid anhydride under 4-dimethylaminopyridine (DMAP) and Et_3N in dry CH_2Cl_2 (Scheme 1). The derivatives **3a-4e** were hydrolyzed in the presence of KOH to furnish derivatives **5a-6g** (Scheme 1). All the acylated products were purified from the reaction mixture by silica gel column chromatography, and the structures were confirmed by ^{1}H-NMR, ^{13}C-NMR and MS analysis. Compounds **2a** and **2g** were prepared according to the published literature [32,33].

2.3. In vitro inhibition of ACE

In vitro ACE inhibition of the newly synthesized analogues were evaluated using colorimetric method [55,56]. The derivatives **2e**, **3b**, pyxinol and standard drug Lisinopril and Enalapril were carried out at 1 μM. Two derivatives **2e** (90.31 %) and **3b** (87.02 %) displayed similar activity with Lisinopril (89.17 %) and superior to pyxinol (57.23 %). Furthermore, the IC_{50} values for derivatives **2e**, **3b**, Lisinopril and Enalapril were calculated from dose-response curves obtained by plotting the percentage inhibition verses the concentration (Fig. 3). IC_{50} values of **2e**, **3b**, Lisinopril and Enalapril were 105 nM, 114 nM, 81 nM and 117 nM, respectively.

2.4. In vitro cytotoxicity

The cytotoxicity evaluation for most potent compounds **2e** and **3b** were assessed towards rat cardiomyoblast cell line (H9c2) as previous literatures described [57–60]. H9c2 cells were treated with increasing doses (5, 10, 25, 50, 100 μM) of compounds **2e** and **3b**. Cell viability of H9c2 cells was determined by cell counting kit-8 (CCK8). As shown in Fig. 4, no toxic effect of compounds **2e** and **3b** on H9c2 cells was observed after 24 h incubation.

2.5. Molecular docking

In order to further understand the ACE-ligand binding mode, the active compounds **2e** and **3b** were docked on to ACE (PDB ID: 1O8A) using Autodock Tools-1.5.6 software. Docking results showed that the ester group of **2e** exhibited strong hydrogen bonding interactions with Tyr523 (2.0 Å), His513 (2.1 Å) and His353 (1.8 Å) in S1 and S2 subsites and closed to the catalytic zinc ion with the distance of 3.4 Å. We also demonstrated that Arg522 (2.2 Å, 2.7 Å) in S2 subsite forms two strong H-bonds interaction with the hydroxyl group at C-25 position with a binding energy (ΔG) of -9.54 kcal/mol (Fig. 5B). The ester group at C-12 position, carbonyl group at C-25 position and oxygen atom in furan ring of compound **3b** formed four strong H-bonds with Arg522 (1.9 Å, 2.3 Å, 2.1 Å, 2.3 Å) in S2 subsite. The carbonyl group at C-3 position also formed H-bond with Ser355 (2.3 Å) in S1 subsite and the distance to zinc ion was 4.4 Å with a binding energy value of -9.6 kcal/mol (Fig. 5C). These results are consistent with the possible ACE inhibition activity of these compounds.

Furthermore, to recognize the inhibitory selectivity of **2e** and **3b**, the N-domain of ACE crystal structure (PDB: 3NXQ) was also used. The inhibitory constant (*Ki*) and binding energy (ΔG) value of compounds **2e** (*Ki* = 102.27 nM, ΔG = -9.54 kcal/mol) and **3b** (*Ki* = 91.65 nM, ΔG = -9.6 kcal/mol) obtained by ACE C-domain were higher than the N-domain (**2e**: *Ki* = 4.48 μM and ΔG = -7.3 kcal/mol, **3b**: *Ki* = 8.60 μM and ΔG = -6.91 kcal/mol), it is divulged that the derivatives **2e** and **3b** had a prosperous inhibitory selectivity towards ACE C-domain rather than ACE N-domain.

2.6. In vivo anti-heart failure activity

The NOAEL were all 100 μg/mL for all the derivatives and pyxinol. After a 4 h treatment, compounds **2e** and **3b** at 1 μg/mL displayed significant activity and similar to Enalapril. Compounds **2e** and **3b** significantly reduced heart dilatation and venous congestion (Table 1 and Fig. 6), while increasing cardiac output as well as heart rate (Table 1).

Compounds **2e** and **3b** also significantly increased the ejection fraction (Fig. 7A) and fractional shortening (Fig. 7B) in a dose-dependent manner (0.5, 1 and 10 μg/mL), and the level of increase by **2e** and **3b** was similar to that observed with the positive control Enalapril.

The results indicate that a caproic acid ester at C-3 position and propionic acid ester at C-3, C-12 and C-25 might play a key role for the binding of the active derivatives with the target receptor in heart failure.

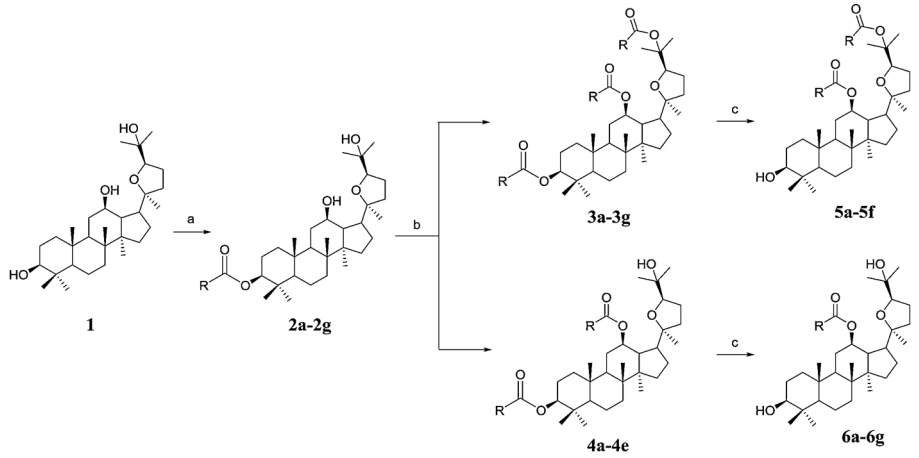

2a R = CH_3 **3a** R = CH_3 **4a** R = $(CH_2)_2CH_3$ **5a** R = CH_3 **6a** R = CH_3
2b R = CH_2CH_3 **3b** R = CH_2CH_3 **4b** R = $(CH_2)_3CH_3$ **5b** R = CH_2CH_3 **6b** R = CH_2CH_3
2c R = $(CH_2)_2CH_3$ **3c** R = $(CH_2)_2CH_3$ **4c** R = $(CH_2)_4CH_3$ **5c** R = $(CH_2)_2CH_3$ **6c** R = $(CH_2)_2CH_3$
2d R = $(CH_2)_3CH_3$ **3d** R = $(CH_2)_3CH_3$ **4d** R = $(CH_2)_5CH_3$ **5d** R = $(CH_2)_3CH_3$ **6d** R = $(CH_2)_3CH_3$
2e R = $(CH_2)_4CH_3$ **3e** R = $(CH_2)_4CH_3$ **4e** R = $(CH_2)_6CH_3$ **5e** R = $(CH_2)_4CH_3$ **6e** R = $(CH_2)_4CH_3$
2f R = $(CH_2)_5CH_3$ **3f** R = $(CH_2)_5CH_3$ **5f** R = $(CH_2)_5CH_3$ **6f** R = $(CH_2)_5CH_3$
2g R = $(CH_2)_6CH_3$ **3g** R = $(CH_2)_6CH_3$ **6g** R = $(CH_2)_6CH_3$

Scheme 1. Synthesis of pyxinol derivatives **2b-2f**, **3a-3 g**, **4a-4e**, **5a-5f** and **6a-6 g**. Reagents and conditions: (a). anhydride, CH_2Cl_2, DMAP, Et_3N, 0 ℃-rt, 4 h; (b). anhydride, CH_2Cl_2, DMAP, Et_3N, 0 ℃-50 ℃, 24 h; (c). ethanol, KOH, rt, 24 h.

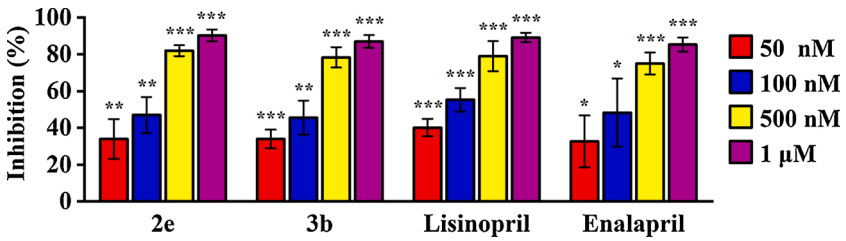

Fig. 3. Dose Response Curves of compounds **2e**, **3b** with ACE inhibiton activity. Data are presented as means ± SD ($n = 3$). *$p < 0.05$, **$p < 0.01$, ***$p < 0.001$ *vs* control.

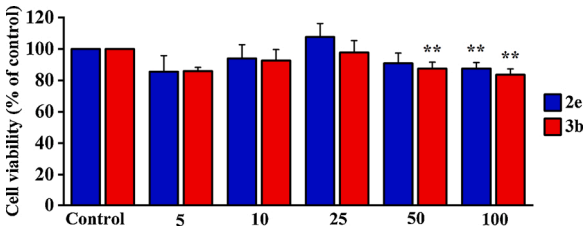

Fig. 4. Cell viability of H9c2 cells treated with different concentrations of **2e** and **3b** for 24 h, respectively. Data are presented as means ± SD ($n = 3$). **$p <$ 0.01 *vs* control.

2.7. Metabolomics study

2.7.1. Validation of UPLC-QTOF-MS

The metabolic characteristics under two modes (ESI + and ESI-) of the model group, control group and **2e** (1 μg/mL) group were identified using UPLC-QTOF-MS. Here, the typical base peak intensity (BPI) chromatograms of zebrafish embryos are shown in Fig. 8. During the entire sequence, the QC (quality control) samples were used to evaluate the system stability. Additionally, eight ions, selected in different spectral regions, were monitored. The exact mass/retention time pairs of these ions in zebrafish embryos were: *m/z* 188.0721, 1.50 min; *m/z* 455.2909, 10.26 min; *m/z* 415.2123, 14.40 min; *m/z* 496.3401, 18.17 min; *m/z* 477.394, 20.65 min; *m/z* 485.2907, 21.40 min; *m/z* 637.3056, 23.27 min; *m/z* 338.3434, 27.46 min in ESI + mode; and *m/z* 203.0489, 0.62 min; *m/z* 197.0012, 4.69 min; *m/z* 242.1744, 9.91 min; *m/z* 265.1481, 16.03 min; *m/z* 566.3474, 18.70 min; *m/z* 480.3084, 20.68 min; *m/z* 681.2971, 23.28 min; *m/z* 850.5622, 26.21 min in ESI- mode. The relative standard deviations (RSDs) of the retention times and the peak areas of the selected ions were 0.16–4.03 % and 0.29–6.34 %, respectively.

The QC samples were used to assess the injection precision. For the eight ions, the RSDs of peak areas in ESI + and ESI- modes were 0.56–1.99 % and 0.19–2.84 %, respectively. And the RSDs of retention times were 0.07−0.51% and 0.03−0.45%, respectively. Five parallel replicate samples of Zebrafish embryos were used to evaluate the reproducibility of sample preparation. The RSDs of the retention time and peak areas were 0.11–1.07 % and 1.62–2.86 % in ESI+, while 0.06−0.58% and 0.23–3.46 % in ESI-. One sample, placed at the same temperature (10 ℃) for different times (0, 2, 4, 8, and 12 h), was used to evalutate the post-preparation stability. The RSDs of the retention times

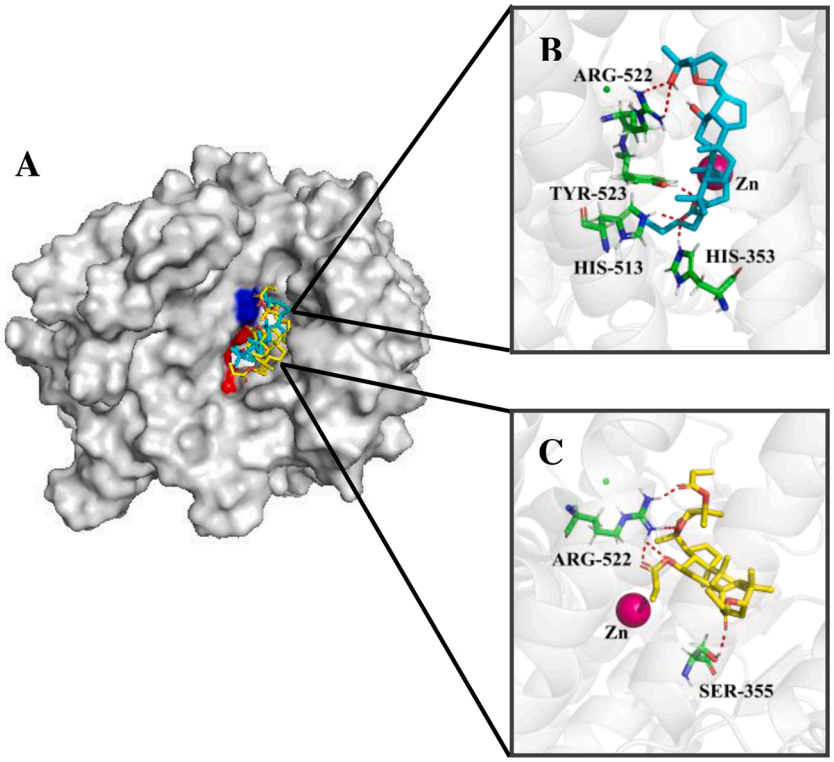

Fig. 5. (A) Docking poses for compound **2e** in cyan, **3b** in yellow, on ACE (PDB: 1O8A). Identical residues were shown in blue and different residues in red. (B) Binding mode of compound **2e**. (C) Binding mode of compound **3b**. Green sticks: residues involved in the interactions; Red dashed lines: hydrogen bonds; Magenta sphere: catalytic zinc ion. (For interpretation of the references to colour in the Figure, the reader is referred to the web version of this article).

Table 1
Efficacy of **2e**, **3b** and the positive control Enalapril (1 μg/mL) on zebrafish heart failure.

Sample	Efficacy on heart rate (%)	Efficacy on heart dilatation (%)	Efficacy on venous congestion (%)	Efficacy on cardiac output (%)
2e	46.69 ± 11.14[b]	33.36 ± 7.55[b]	39.51 ± 7.32[c]	61.74 ± 12.78[b]
3b	40.08 ± 11.29[b]	50.00 ± 4.84[c]	47.95 ± 4.54[c]	63.44 ± 13.60[b]
Enalapril	41.24 ± 4.68[c]	52.72 ± 10.51[c]	21.67 ± 7.01[b]	74.51 ± 8.608[c]

[a]Data are presented as means ± SD ($n = 3$). [b]$^{**}p < 0.01$, [c]$^{***}p < 0.001$ *vs* model.

and peak areas were 0.09−0.59% and 1.66–5.00 % in ESI+, while 0.34–1.05 % and 0.52–4.76 % in ESI-. Therefore, both precision, reproducibility and stability of the entire experimental performances were good and acceptable.

2.7.2. *Identification of the differential metabolites and metabolic pathways*

In the present study, the PCA, OPLS-DA and S-plot were obtained by using pareto-scaling technique. As shown in PCA score polts (Fig. 9A, each spot represented a sample): The QC injections were clusterly located in the middle of three groups, meaning the system exhibited well stability; the samples from three groups were generally clustered, indicating each group existed similarity; three groups were seperated, meaning that these groups could be easily differentiated. Additionally, the **2e** group was located between the model and control group, indicating that **2e** could improve the metabolic disorders in HF zebrafish. In

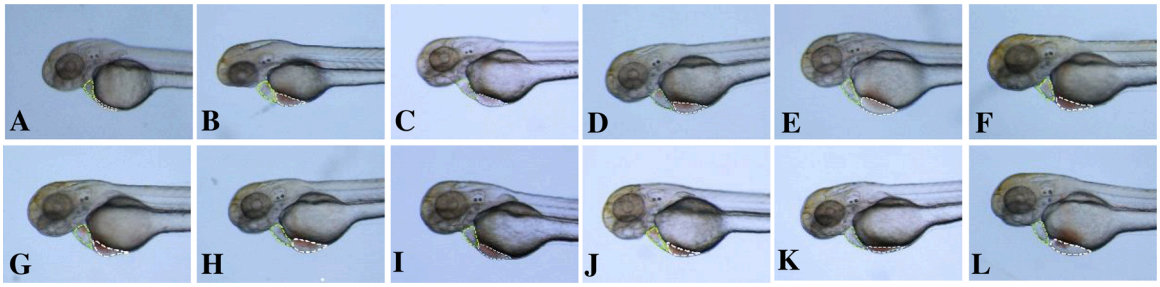

Fig. 6. Heart and veins in Zebrafish. (A) zebrafish control group; (B) zebrafish heart failure model; (C-E) treated with **2e**, **3b** and pyxinol at 0.5 μg/mL; (F-I) treated with **2e**, **3b**, pyxinol and Enalapril at 1 μg/mL; (J-L) treated with **2e**, **3b** and pyxinol at 10 μg/mL. Green dotted line: Heart and heart dilatation; white dotted line: veins and venous congestion. (For interpretation of the references to colour in the Figure, the reader is referred to the web version of this article).

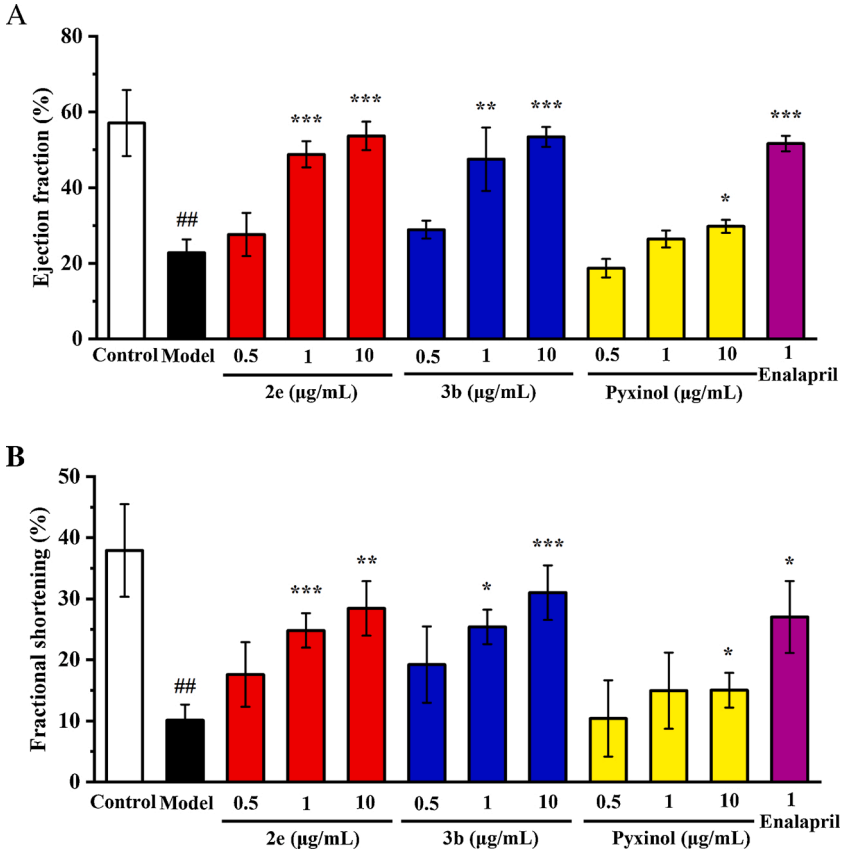

Fig. 7. The effect of compounds **2e**, **3b** and pyxinol on ejection fraction and fractional shortening in the zebrafish heart failure model at 0.5, 1, 10 μg/mL and Enalapril at 1 μg/mL. **(A)** The effect on ejection fraction. **(B)** The effect on fractional shortening. Data were expressed as mean ± SD and percentage of control value ($n = 3$). $^{###}p < 0.001$, $^{##}p < 0.01$ *vs* control; $^{***}p < 0.001$, $^{**}p < 0.01$, $^{*}p < 0.05$ *vs* model group.

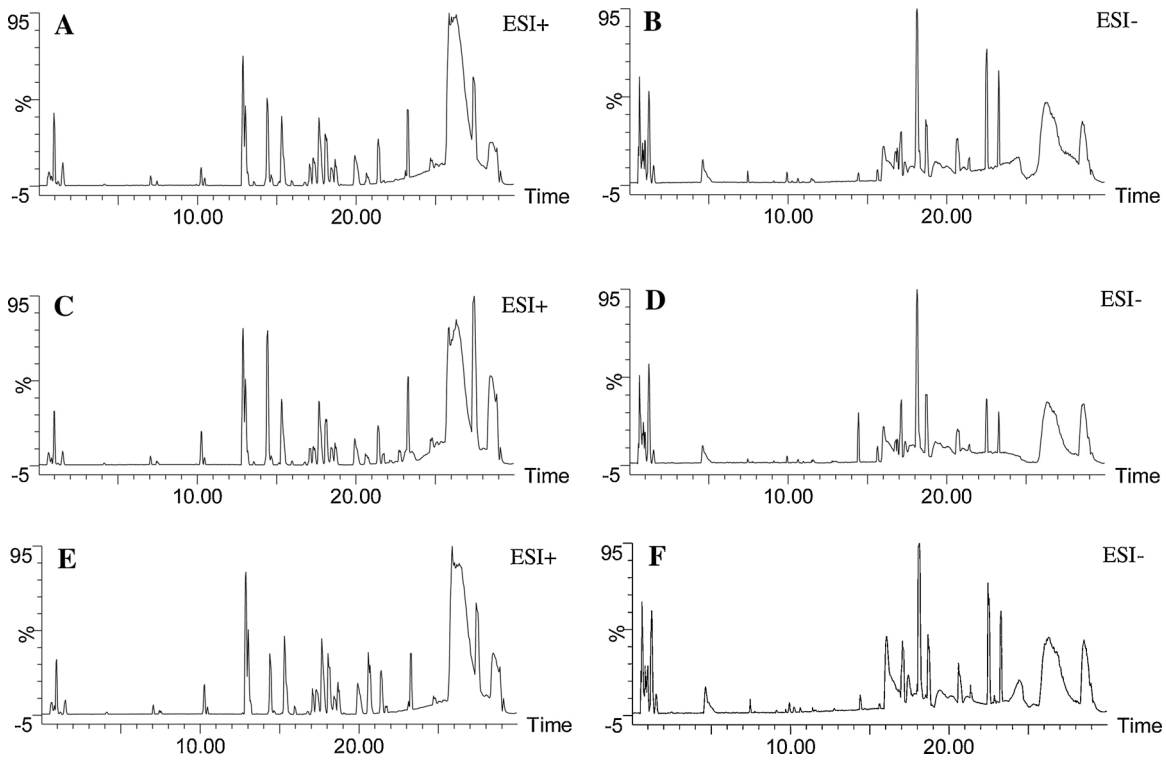

Fig. 8. The typical BPI chromatograms of control group (A,B), model group (C,D) and **2e** group (E,F).

order to uncover the metabolic biomarkers, OPLS-DA (Fig. 9B, one spot represented one sample) was applied to compare metabolic changes between model group and **2e** group. Validation of the OPLS-DA is typically described by R2 and Q2, which was performed by permutation testing. As shown in Fig. 9C, all Q2-values to the left were lower than the original points to the right, indicating that the model displayed good prediction ability and reliability. From the S-plots (Fig. 9D), the spots (represented a variable), located on the outer ends of the S-shaped point swarm, were regarded as the differential metabolites. Thus, combined S-plots, the VIP value (VIP $>$ 1) and the *t*-test ($p < 0.05$), a total of 25 robust endogenous metabolites were identified as potential biomarkers (marked in red in S-plots) in samples (Table 2).

Receiver operating characteristic (ROC) curves were used to evaluate the specificity and sensitivity of biomarkers. If the area under the curve (AUC) is greater than 0.7, the biomarkers can be employed as diagnostic biomarkers. In our study, 25 metabolites whose AUC was greater than 0.8 were considered the potential diagnostic markers for heart failure and contributed to **2e** treatment (Fig. 10**A** and **B**, Table 3). The heatmap (Fig. 11) generated could visualize and characterize the metabolic differences of the biomarkers in three groups; green represented low abundance and red represented high abundance. As shown in Fig. 12 (size of each spot represented the influence in this pathway), the metabolic network showed that **2e** could regulate the 8 pathways (Table 4) were as follows:

2.7.2.1. Arachidonic acid metabolism. Arachidonic acid, an omega-6 polyunsaturated fatty acid, mediates inflammation and the functioning heart [61]. The disturbance of arachidonic acid and its metabolites are often related to the development of cardiovascular diseases, such as HF [62] and anti-arachidonic acid metabolism could improve myocardial infraction and HF [63]. Prostaglandin E2 (PGE2), synthesized from arachidonic acids [64], could reduces cardiac contractility *via* EP3 receptor and its increase will aggravate HF [65]. Additionally, arachidonic acid can be oxidated to generate 15(S)-HPETE, which are then reduced to 15-HETE [66,67]. In this study, the levels of arachidonic acid, leukotriene B4, 15-HETE and PGE2 increased in the model group compared with 2e group. The result is consistent with the previous study in alleviation of HF [68].

2.7.2.2. Lipid metabolism. It is closely related to the onset and development of HF [69]. Here, two kinds of lipid metabolism detected were: i) *Glycerophospholipid metabolism:* The observed increase in contents of LysoPC (18:1(9Z)) in the model group could be attributed to the risk of HF [70]. Choline is an essential nutrient for humans [71]. Choline is metabolized to Trimethylamine N-oxide (TMAO), which could exacerbate cardiac dysfunction and myocardial hypertrophy in a model of cardiovascular disease [72,73]. ii) *Linoleic acid metabolism:* reduced level of linoleic acid were observed in the model group, indicating HF could perturb linoleic acid metabolism. Prior studies have noted the importance of linoleic acid, namely high levels of linoleic acid may improving cardiac malfunction and mitochondrial function in heart failure [74]. iii) *Sphingolipid metabolism:* Sphinganine, the member of sphingolipid metabolite family, have attracted much attention in the pathophysiology of the heart [75]. It could phosphorylate and degrade the sphinganine 1-phosphate, which exhibit the potent cardioprotective activity [76]. In this study, the level of sphinganine was down-regulated in the model group but up-regulated in the **2e** group.

2.7.2.3. Folate biosynthesis. Until now, there was no literature have been reported the relationship between folate biosynthesis and HF. In this experiment, levels of dihydrobiopterin and dyspropterin were decreased in the HF model group, indicating that HF could cause folate biosynthesis to be perturbed.

2.7.2.4. Pyruvate metabolism. Pyruvate metabolism is a potential target for therapy in heart failure [77]. Pyruvate, the end-product of glycolysis, is critical for mitochondrial ATP generation in mitochondria by oxidative phosphorylation [78]. It could produce lactic acid *via* the enzyme lactate dehydrogenase [62]. In this study, the levels of pyruvate and L-lactic acid were increased in the model group. After treatment with **2e**, the levels of pyruvate and L-lactic acid all showed a tendency for returning to baseline values in the **2e** group

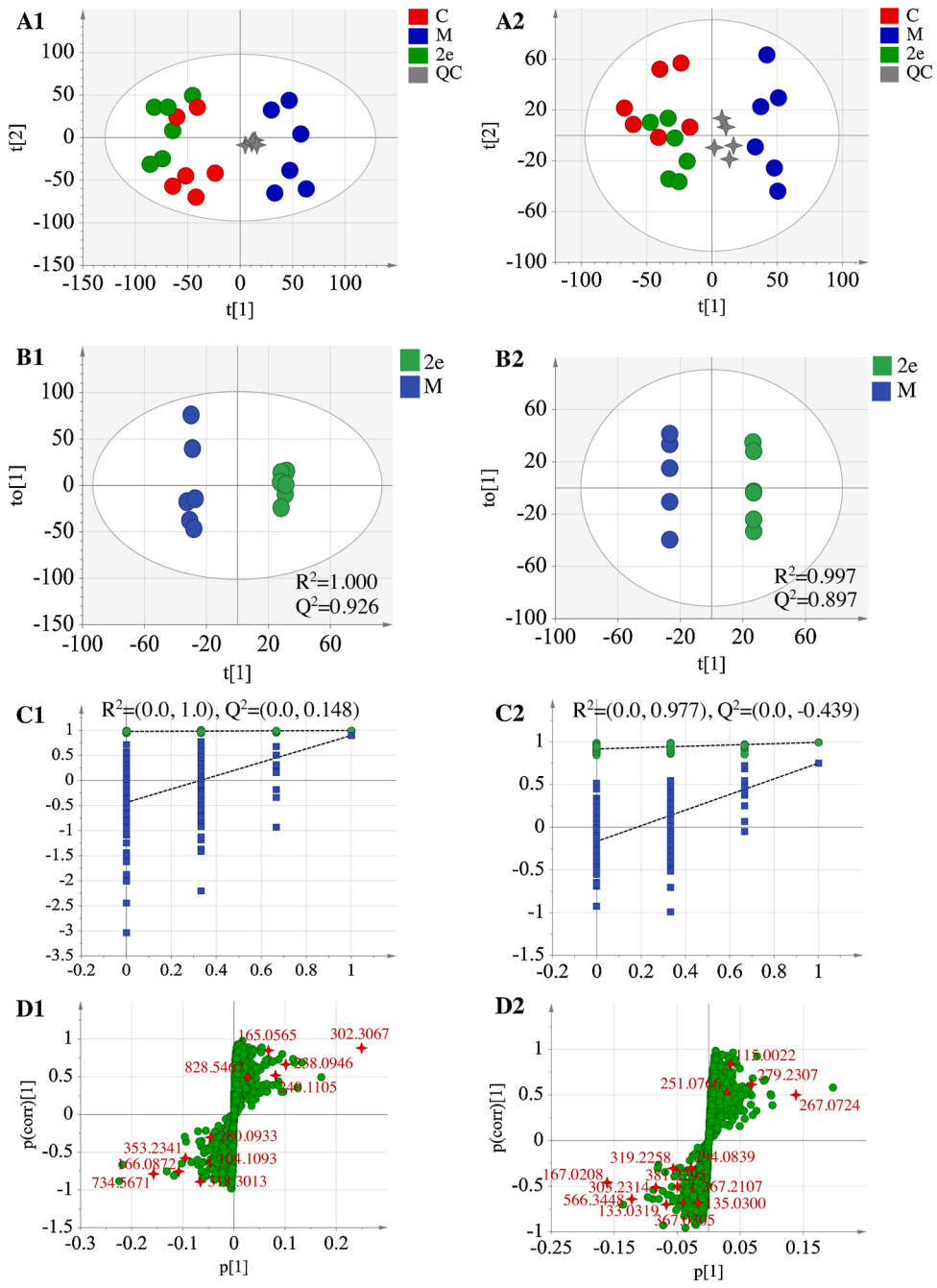

Fig. 9. (A) PCA score plots of control, model and **2e** groups and (B/C/D) OPLS-DA/Permutation test/S-plots of model and **2e** groups in ESI + mode (A1/B1/C1/D1) and ESI- (A2/B2/C2/D2). "M" represents model group; "C" represents control group.

2.7.2.5. Phenylalanine metabolism. The phenylalanine level was markedly elevated in the model group, meaning the disorder of phenylalanine metabolism, which is consistent with previous studies, patients with elevated phenylalanine levels exhibited incompletely metabolized waste of fatty acids in the circulation and dysfunctional energy production machinery [79]

2.7.2.6. Purine metabolism. Uric acid, the final product of purine metabolism, exhibit anti-oxidation, maintaining blood pressure and anti-aging activity [80]. In this study, elevated levels of uric acid was observed in the model group. This is in accordance with previous studies, increased uric acid is a feature of inflammation and oxidative stress in heart failure [81].

3. Materials and methods

3.1. Materials and reagents

All commercial chemicals and solvents were of analytical grade and were used without further purification unless otherwise stated. Thin-layer chromatography (TLC) was used to monitor the reaction progress. The NMR spectra were taken in $CDCl_3$ on Bruker AV-600 spectrometer (Bruker Co., Karlsruhe, Germany) with TMS as internal standard. HR-ESI-MS was performed on Waters Xevo G2-XS QTOF mass spectrometer (Waters Co., Milford, MA, USA). Both methanol and acetonitrile were of UPLC-MS pure grade obtained from Fisher Chemical Company (Geel, Belgium). Deionized water was prepared by using Millipore water purification system (Millipore, Billerica, MA, USA).

Table 2
Distinct metabolites identified in Zebrafish embryos samples.

No.	RT (min)	Mass	Compound name	VIP value	Formula	Adducts	Δm (ppm)	HMDB ID	Pathways	Content level
1*	0.58	104.1093	Choline	1.44	$C_5H_{14}NO$	M+H	4.92	HMDB0000097	GlyM	$C_M > C_C > C_D$
2[a]	0.59	280.0933	Glycerophosphocholine	1.41	$C_8H_{20}NO_6P$	M + Na	4.49	HMDB0000086	GlyM	$C_M > C_C > C_D$
3[a]	0.63	115.0022	Fumaric acid	2.09	$C_4H_4O_4$	M-H	−3.90	HMDB0000134	PyM	$C_M < C_D < C_C$
4[a]	0.65	133.0139	Pyruvate	4.72	$C_3H_4O_3$	M + FA-H	−2.59	HMDB0000243	PyM	$C_M > C_D > C_C$
5*	0.66	167.0208	Uric acid	13.67	$C_5H_4N_4O_3$	M-H	−1.58	HMDB0000289	PM	$C_M > C_D > C_C$
6[a]	0.68	240.1105	Dihydrobiopterin	4.11	$C_9H_{13}N_5O_3$	M+H	2.77	HMDB0000038	FB	$C_M < C_D < C_C$
7[a]	0.74	362.0503	Cyclic pyranopterin monophosphate	2.97	$C_{10}H_{14}N_5O_8P$	M-H	−1.17	HMDB0059639	FB	$C_M > C_D > C_C$
8[a]	0.75	135.0300	L-Lactic acid	1.61	$C_3H_6O_3$	M + FA-H	0.78	HMDB0000190	PyM	$C_M > C_C > C_D$
9[a]	0.79	251.0766	Deoxyinosine	1.77	$C_{10}H_{12}N_4O_4$	M-H	−4.88	HMDB0000071	PM	$C_M < C_D < C_C$
10[a]	0.80	165.0565	Phenylpyruvic acid	3.51	$C_9H_8O_3$	M+H	3.39	HMDB0000205	PheM	$C_M < C_D < C_C$
11[a]	0.80	267.0724	Inosine	9.87	$C_{10}H_{12}N_4O_5$	M-H	−4.10	HMDB0000195	PM	$C_M < C_C < C_D$
12[a]	0.83	238.0946	Dyspropterin	5.20	$C_9H_{11}N_5O_3$	M+H	4.77	HMDB0001195	FB	$C_M < C_C < C_D$
13*	0.94	166.0872	L-Phenylalanine	6.65	$C_9H_{11}NO_2$	M+H	2.69	HMDB0000159	PheM	$C_M > C_C > C_D$
14[a]	1.20	294.0839	S-Acetyldihydrolipoamide-E	1.90	$C_{10}H_{19}NO_2S_2$	M + FA-H	−0.07	HMDB0006878	PyM	$C_M > C_C > C_D$
15[a]	9.13	367.2107	Prostaglandin G2	1.74	$C_{20}H_{32}O_6$	M-H	−2.21	HMDB0003235	AM	$C_M > C_C \approx C_D$
16[a]	15.33	302.3067	Sphinganine	11.46	$C_{18}H_{39}NO_2$	M+H	4.45	HMDB0000269	SphM	$C_M < C_D < C_C$
17[a]	15.58	318.3013	Phytosphingosine	2.69	$C_{18}H_{39}NO_3$	M+H	3.24	HMDB0004610	SphM	$C_M > C_C \approx C_D$
18*	17.36	319.2258	15-HETE	3.22	$C_{20}H_{32}O_3$	M-H	−4.48	HMDB0003876	AM	$C_M > C_C > C_D$
19[a]	18.12	353.2341	Prostaglandin E2	5.63	$C_{20}H_{32}O_5$	M+H	2.24	HMDB0001220	AM	$C_M > C_C \approx C_D$
20[a]	18.26	566.3448	LysoPC(18:1(9Z)/0:0)	9.93	$C_{26}H_{52}NO_7P$	M + FA-H	−2.72	HMDB0002815	GlyM	$C_M > C_C > C_D$
21[a]	21.53	381.2295	Leukotriene B4	3.20	$C_{20}H_{32}O_4$	M + FA-H	3.25	HMDB0001085	AM	$C_M > C_D > C_C$
22[a]	22.86	828.5467	lactosylceramide	1.99	$C_{42}H_{79}NO_{13}$	M + Na	2.82	HMDB0004866	SphM	$C_M < C_D < C_C$
23*	22.90	303.2314	Arachidonic acid	5.01	$C_{20}H_{32}O_2$	M-H	−2.12	HMDB0001043	AM	$C_M > C_C > C_D$
24*	23.20	279.2307	Linoleic acid	4.19	$C_{18}H_{32}O_2$	M-H	−3.07	HMDB0000673	LM	$C_M < C_D \approx C_C$
25[a]	25.74	734.5671	PC(16:0/16:0)	7.20	$C_{40}H_{80}NO_8P$	M+H	−3.17	HMDB0000564	AM, LM	$C_M > C_C \approx C_D$

RT, Retention Time, min; Mass, Measured mass, Da; Δm, Relative Deviation, ppm; * Metabolites validated with standards; [a] Metabolites confirmed by MS/MS fragments; "D" represents drug intervention group (**2e** group); "M" represents model group.

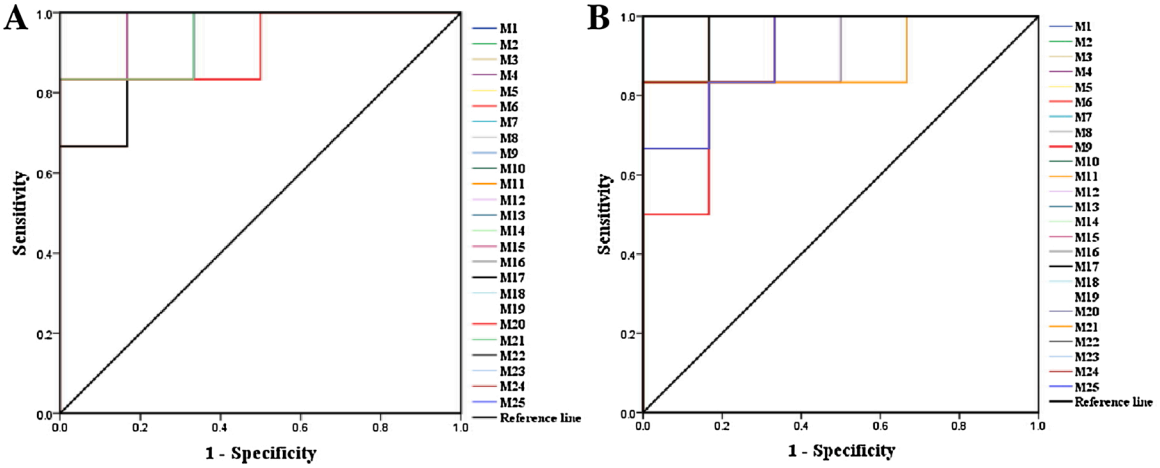

Fig. 10. The ROC curves generated using 25 biomarkers contributing to (A) heart failure progress between the model group and the control group, (B) **2e** treatment between the model group and **2e** group (the numbers are consistent with No. in Table 3).

Formic acid (UPLC-grade) was bought from Sigma Aldrich. All other chemicals were of analytical grade.

*3.1.1. General procedure for the preparation of **2a-2g***

To a stirred solution of compound **1** (1.05 mmol) in CH_2Cl_2 were added DMAP (0.40 mmol) and Et_3N (1.58 mmol) successively, and then cooled to 0℃. The corresponding acid anhydride (1.58 mmol) was added slowly, and allowed the temperature of the reaction solution warm to room temperature. After the reaction is completed, extracted with ethyl acetate (3 × 10 mL) and the organic layers was washed by saturated $NaHCO_3$ (3 × 10 mL), water (3 × 10 mL) and saturated brine (3 × 10 mL) successively, dried over anhydrous Na_2SO_4 and evaporated. The residue was purified by column chromatography (*n*-hexane: ethyl acetate) to afford compounds **2a-2g**.

*3.1.1.1. (20S, 24R)-epoxy-3β-O-acetyl-dammarane-12β, 25-diol (**2a**).* White solid, yield 85 %, ^{1}H NMR (600 MHz, $CDCl_3$) δ 5.56 (s, 1 H), 4.48−4.45 (m, 1 H), 3.85−3.83 (m, 2 H), 3.53−3.49 (m, 1 H), 2.20−2.14 (m, 1 H), 2.04 (s, 3 H), 2.02−1.95 (m, 1 H), 1.91−1.83 (m, 3 H), 1.72−1.41 (m, 13 H), 1.32−1.28 (m, 2 H), 1.27 (s, 3 H), 1.26 (s, 3 H), 1.13−1.11 (m, 1 H), 1.09 (s, 3 H), 1.06−1.03 (m, 1 H), 0.98 (s, 3 H), 0.89 (s, 3 H), 0.87 (s, 3 H), 0.84 (s, 6 H). ^{13}C NMR (150 MHz, $CDCl_3$) δ 171.0, 86.5, 85.4, 80.8, 71.0, 70.1, 56.1, 52.0, 50.4, 49.4, 48.0, 39.8, 38.7, 37.9, 37.1, 34.8, 32.6 (2C), 31.3, 31.2, 28.6, 27.9, 27.9, 27.6, 26.2, 25.0, 23.7, 21.3, 18.2 (2C), 16.4, 15.4. HR-ESI-MS *m/z* for $C_{32}H_{55}O_5$ $[M+H]^+$: calcd., 519.3971; found: 519.3955.

*3.1.1.2. (20S, 24R)-epoxy-3β-O-propionyl-dammarane-12β, 25-diol (**2b**).* White solid, yield 73.3 %, ^{1}H NMR (600 MHz, $CDCl_3$) δ 5.60 (s, 1 H), 4.51−4.48 (m, 1 H), 3.91 (s, 1 H), 3.88−3.85 (m, 1 H), 3.56−3.51 (m, 1 H), 2.37−2.32 (m, 2 H), 2.23−2.19 (m, 1 H), 2.10−1.97 (m, 2 H), 1.94−1.85 (m, 3 H), 1.74−1.41 (m, 11 H), 1.35−1.33 (m, 1 H), 1.31 (s, 1

Table 3
The area under curve (AUC) values and *p* values of the biomarkers in two predictive ROC curves.

No.	M and N		M and **2e**	
	AUC	*p*	AUC	*p*
1	0.972	<0.01	0.944	<0.01
2	1.000	<0.01	1.000	<0.001
3	0.944	<0.01	0.944	<0.01
4	0.944	<0.01	0.917	<0.01
5	1.000	<0.01	0.944	<0.01
6	0.944	0.01	0.944	<0.01
7	0.972	<0.01	1.000	<0.001
8	0.944	<0.01	0.972	<0.01
9	0.972	<0.01	0.917	<0.01
10	0.944	<0.01	1.000	<0.01
11	0.944	<0.01	0.972	<0.01
12	0.972	<0.01	0.944	<0.01
13	0.944	0.01	0.972	<0.01
14	0.944	<0.01	0.972	<0.01
15	0.972	0.01	0.917	0.01
16	1.000	<0.01	0.972	<0.01
17	0.944	0.02	0.944	<0.01
18	1.000	<0.01	1.000	<0.001
19	1.000	<0.01	1.000	<0.001
20	0.917	0.02	0.917	<0.01
21	0.944	<0.01	0.889	<0.01
22	1.000	<0.01	0.944	<0.01
23	1.000	0.02	0.972	<0.01
24	1.000	0.01	0.944	<0.01
25	0.944	0.01	0.917	<0.01

H), 1.30 (s, 3 H), 1.29 (s, 3 H), 1.27 (s, 1 H), 1.18−1.15 (m, 3 H), 1.13 (d, *J* =5.0 Hz, 1 H), 1.11 (s, 3 H), 1.09−1.06 (m, 1 H), 1.00 (s, 3 H), 0.92 (s, 3 H), 0.90 (s, 3 H), 0.87 (s, 3 H), 0.86 (s, 3 H). ^{13}C NMR (150 MHz, $CDCl_3$) δ 174.3, 86.5, 85.4, 80.5, 70.9, 70.1, 56.1, 52., 50.4, 49.4, 47.9, 39.7, 38.6, 37.9, 37.1, 34.7, 32.6, 31.3, 31.2, 28.6, 28.1, 27.9, 27.9, 27.6, 26.1, 25.00, 23.7, 18.2 (2C), 16.4, 16.4, 15.4, 9.3. HR-ESI-MS *m/z* for $C_{33}H_{57}O_5$ $[M+H]^+$: calcd., 533.4128; found: 533.4146.

3.1.1.3. (20S, 24R)-epoxy-3β-O-butyryl-dammarane-12β, 25-diol ***(2c)***. White solid, yield 60.6 %, ^{1}H NMR (600 MHz, $CDCl_3$) δ 5.59 (s, 1 H), 4.50−4.46 (m, 1 H), 3.90 (s, 1 H), 3.87−3.84 (m, 1 H), 3.54−3.49 (m, 1 H), 2.28 (t, *J* =10.0 Hz, 2 H), 2.22−2.17 (m, 1 H), 2.08−1.95 (m, 2 H), 1.92−1.84 (m, 3 H), 1.73−1.40 (m, 14 H), 1.33−1.30 (m, 2 H), 1.28 (s, 3 H), 1.27 (s, 3 H), 1.14−1.11 (m, 1 H), 1.10 (s, 3 H), 1.07−1.04 (m, 1 H), 0.99 (s, 3 H), 0.95 (t, *J* =10.0 Hz, 3 H), 0.90 (s, 3 H), 0.88 (s, 3 H), 0.85 (s, 3 H), 0.84 (s, 3 H). ^{13}C NMR (150 MHz, $CDCl_3$) δ 173.5, 86.5, 85.4, 80.4, 70.9, 70.1, 56.0, 52.0, 50.4, 49.4, 47.9, 39.7, 38.6, 37.9, 37.1, 36.7, 34.7, 32.6, 31.3, 31.2, 28.6, 27.9, 27.9, 27.6, 26.1, 25.00, 23.7, 18.6, 18.2 (2C), 16.4, 16.4, 15.4, 13.7. HR-ESI-MS *m/z* for $C_{34}H_{59}O_5$ $[M+H]^+$: calcd., 547.4284; found: 547.4301.

3.1.1.4. (20S, 24R)-epoxy-3β-O-valeryl-dammarane-12β, 25-diol ***(2d)***. White solid, yield 48.9 %, ^{1}H NMR (600 MHz, $CDCl_3$) δ 5.59 (s, 1 H), 4.49−4.46 (m, 1 H), 3.89 (s, 1 H), 3.87−3.84 (m, 1 H), 3.54−3.49 (m, 1 H), 2.30 (t, *J* =10.0 Hz, 2 H), 2.22−2.17 (m, 1 H), 2.08−1.95 (m, 2 H), 1.92−1.84 (m, 3 H), 1.75−1.44 (m, 14 H), 1.39−1.30 (m, 4 H), 1.28 (s, 3 H), 1.27 (s, 3 H), 1.14−1.11 (m, 1 H), 1.10 (s, 3 H), 1.07−1.03 (m, 1 H), 0.99 (s, 3 H), 0.93 (s, 1 H), 0.92 (s, 2 H), 0.90 (s, 3 H), 0.88 (s, 3 H), 0.85 (s, 3 H), 0.84 (s, 3 H). ^{13}C NMR (150 MHz, $CDCl_3$) δ 173.6, 86.5, 85.4, 80.4, 70.9, 70.1, 56.0, 52.0, 50.4, 49.4, 47.9, 39.7, 38.6, 37.9, 37.1, 34.8, 34.5, 32.6, 31.3, 31.2, 28.6, 27.9, 27.9, 27.6, 27.2, 26.1, 25.00, 23.7, 22.3, 18.2 (2C), 16.5, 16.4, 15.4, 13.7. HR-ESI-MS *m/z* for $C_{35}H_{61}O_5$ $[M+H]^+$: calcd., 561.4441; found: 561.4458.

3.1.1.5. (20S, 24R)-epoxy-3β-O-hexanoyl-dammarane-12β, 25-diol ***(2e)***. White solid, yield 73.3 %, ^{1}H NMR (600 MHz, $CDCl_3$) δ 5.57 (s, 1 H), 4.49−4.46 (m, 1 H), 3.86−3.83 (m, 2 H), 3.54−3.49 (m, 1 H), 2.29 (t, *J* =10.0 Hz, 2 H), 2.21−2.17 (m, 1 H), 2.08−1.95 (m, 2 H), 1.91−1.83 (m, 3 H), 1.72−1.59 (m, 9 H), 1.57−1.52 (m, 2 H), 1.49−1.43 (m, 3 H), 1.35−1.29 (m, 6 H), 1.28 (s, 3 H), 1.27 (s, 3 H), 1.13−1.11 (m, 1 H), 1.09 (s, 3 H), 1.06−1.03 (m, 1 H), 0.98 (s, 3 H), 0.91 (s, 1 H), 0.90 (s, 3 H), 0.89 (s, 2 H), 0.88 (s, 3 H), 0.85 (s, 3 H), 0.84 (s, 3 H). ^{13}C NMR (150 MHz, $CDCl_3$) δ 173.7, 86.5, 85.4, 80.4, 71.0, 70.1, 56.1, 52.0, 50.4, 49.4, 48.0, 39.8, 38.7, 37.9, 37.1, 34.8 (2C), 32.6, 31.4 (2C), 31.2, 29.7, 28.6, 28.0 (2C), 27.6, 26.2, 25.0, 24.9, 23.8, 22.3, 18.2, 16.5, 16.4, 15.4, 13.9. HR-ESI-MS *m/z* for $C_{36}H_{63}O_5$ $[M+H]^+$: calcd., 575.4597; found: 575.4575.

3.1.1.6. (20S, 24R)-epoxy-3β-O-heptanoyl-dammarane-12β, 25-diol ***(2f)***. White solid, yield 53.5 %, ^{1}H NMR (600 MHz, $CDCl_3$) δ 5.58 (s, 1 H), 4.50−4.48 (m, 1 H), 3.89 (s, 1 H), 3.87−3.85 (m, 1 H), 3.55−3.52 (m, 1 H), 2.31 (t, *J* =12.0 Hz, 2 H), 2.22−2.19 (m, 1 H), 2.08−1.98 (m, 2 H), 1.93−1.86 (m, 3 H), 1.73−1.55 (m, 10 H), 1.50−1.44 (m, 3 H), 1.36−1.30 (m, 8 H), 1.29 (s, 3 H), 1.29 (s, 3 H),1.14−1.12 (m, 2 H), 1.11

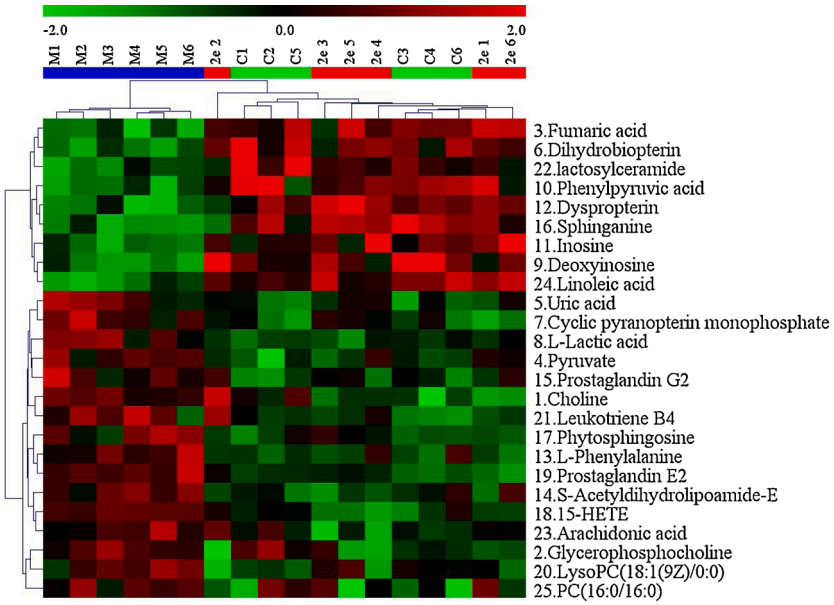

Fig. 11. The heatmap of all potential biomarkers.

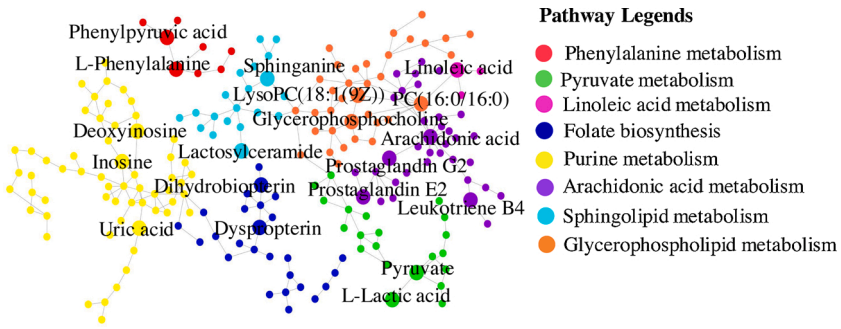

Fig. 12. The metabolic pathways.

Table 4
The results from metabolic pathways of differential metabolites.

Pathway name	Match status	*p*	-log (*p*)	Holm *p*	FDR	Impact
Arachidonic acid metabolism (AM)	23/33	< 0.001	7.8976	< 0.001	< 0.001	0.8694
Phenylalanine metabolism (PheM)	4/8	0.0903	1.0441	1.0000	1.0000	0.6190
Linoleic acid metabolism (LM)	2/4	0.2320	0.6340	1.0000	1.0000	1.0000
Pyruvate metabolism (PyM)	5/22	0.6060	0.2174	1.0000	1.0000	0.4971
Folate biosynthesis (FB)	6/27	0.6250	0.2038	1.0000	1.0000	0.1866
Sphingolipid metabolism (SphM)	4/21	0.7560	0.1214	1.0000	1.0000	0.1582
Glycerophospholipid metabolism (GlyM)	7/38	0.8170	0.0880	1.0000	1.0000	0.4322
Purine metabolism (PM)	7/66	0.9980	0.0010	1.0000	1.0000	0.2744

(s, 3 H), 1.10−1.06 (m, 1 H), 1.00 (s, 3 H), 0.92 (s, 3 H), 0.91−0.89 (m, 6 H), 0.87 (s, 3 H), 0.86 (s,3 H). ^{13}C NMR (150 MHz, $CDCl_3$) δ 173.7, 86.5, 85.4, 80.4, 71.0, 70.1, 56.1, 52.0, 50.4, 49.4, 48.0, 39.8, 38.6, 37.9, 37.1, 34.9, 34.8, 32.6, 31.5, 31.3, 31.2, 28.8, 28.6, 28.0, 27.9, 27.6, 26.2, 25.1, 25.0, 23.7, 22.5, 18.2, 18.2, 16.5, 16.4, 15.4, 14.0. HR-ESI-MS *m/z* for $C_{37}H_{65}O_5$ $[M+H]^+$: calcd., 589.4754; found: 589.4773.

*3.1.1.7. (20S, 24R)-epoxy-3β-O-octanoyl-dammarane-12β, 25-diol (**2g**).* White solid, yield 53.4 %, ^{1}H NMR (600 MHz, $CDCl_3$) δ 5.56 (s, 1 H), 4.48−4.45 (m, 1 H), 3.86 (s, 1 H), 3.85−3.83 (m, 1 H), 3.53−3.48 (m, 1 H), 2.28 (t, *J* =12.0 Hz, 2 H), 2.20−2.16 (m, 1 H), 2.07−1.95 (m, 2 H), 1.90−1.83 (m, 3 H), 1.71−1.41 (m, 15 H), 1.30−1.28 (m, 8 H), 1.27 (s, 3 H), 1.26 (s, 3 H),1.13−1.11 (m, 2 H), 1.09 (s, 3 H), 1.06−1.03 (m, 1 H), 0.98 (s, 3 H), 0.89 (s, 3 H), 0.88 (s, 2 H), 0.87 (s, 3 H), 0.86 (s, 1 H), 0.84 (s, 3 H), 0.83 (s,3 H). ^{13}C NMR (150 MHz, $CDCl_3$) δ 173.7, 86.5, 85.4, 80.4, 71.0, 70.1, 56.1, 52.0, 50.4, 49.4, 48.0, 39.8, 38.6, 37.9, 37.1, 34.8, 34.8, 32.6, 31.7, 31.3, 31.2, 29.1, 28.9, 28.6, 28.0, 27.9, 27.6, 26.1, 25.2, 25.0, 23.7, 22.6, 18.2, 18.2, 16.5, 16.4, 15.4, 14.1. HR-ESI-MS *m/z* for $C_{38}H_{67}O_5$ $[M+H]^+$: calcd., 603.4910; found: 603.4929.

*3.1.2. General Procedure for the Preparation of **3a-3g** and **4a-4e***

To a stirred solution of compound **2a-2g** (1.05 mmol) in CH_2Cl_2 were added DMAP (0.80 mmol) and Et_3N (3.16 mmol) successively, and then cooled to 0℃. The corresponding acid anhydride (3.16 mmol) was added slowly, and allowed the temperature of the reaction solution warm to 50 ℃ and refluxed. After the reaction is completed, extracted with ethyl acetate (3 × 10 mL), and the organic layer was washed by saturated $NaHCO_3$ (3 × 10 mL), water (3 × 10 mL) and saturated brine (3 × 10 mL) successively, dried over anhydrous Na_2SO_4 and evaporated. The residue was purified by column chromatography (*n*-hexane: ethyl acetate) to afford compounds **3a-3g** and **4a-4e.**

*3.1.2.1. (20S, 24R)-epoxy-3β, 12β, 25-O-triacetyl-dammarane (**3a**).* White solid, yield 29.5 %, ^{1}H NMR (600 MHz, $CDCl_3$) δ 4.86−4.81 (m, 1 H), 4.49−4.47 (s, 1 H), 3.88 (t, *J* =12.0 Hz, 1 H), 2.02 (s, 3 H), 2.00 (s, 3 H), 1.96 (s, 3 H), 1.93−1.72 (m, 6 H), 1.69−1.45 (m, 11 H), 1.42 (s, 6 H), 1.30−1.29 (m, 1 H),1.18−1.16 (m, 4 H), 1.12−1.01 (m, 3 H), 0.98 (s, 3 H), 0.92 (s, 3 H), 0.87 (s, 3 H), 0.84 (s, 6 H). ^{13}C NMR (150 MHz, $CDCl_3$) δ 170.9, 170.6, 170.5, 86.0, 83.1, 82.5, 80.6, 75.5, 55.8, 52.2, 50.8, 49.6, 46.2, 39.6, 39.0, 38.5, 37.9, 37.0, 34.4, 31.0, 28.4, 28.0, 27.0, 25.9, 23.6, 22.7, 22.6, 21.9, 21.8, 21.7, 21.3, 18.1, 17.4, 16.5, 16.1, 15.6. HR-ESI-MS *m/z* for $C_{36}H_{59}O_7$ $[M+H]^+$: calcd., 603.4183; found: 603.4160.

*3.1.2.2. (20S, 24R)-epoxy-3β, 12β, 25-O-tripropionyl-dammarane (**3b**).* White solid, yield 25.9 %, ^{1}H NMR (600 MHz, $CDCl_3$) δ 4.88−4.84 (m, 1 H), 4.49 (dd, *J* = 12.0, 6.0 Hz, 1 H), 3.88 (t, *J* =12.0 Hz, 1 H), 2.34−2.21 (m, 6 H), 2.04−1.99 (m, 1 H), 1.93−1.71 (m, 7 H), 1.68−1.45 (m, 12 H), 1.43 (s, 6 H),1.30 (d, *J* =12.0 Hz, 1 H), 1.16 (s, 3 H), 1.14−1.08 (m, 9 H), 1.05−1.01 (m, 1 H), 0.99 (s, 3 H), 0.93 (s, 3 H), 0.87 (s, 3 H), 0.85 (s, 6 H). ^{13}C NMR (150 MHz, $CDCl_3$) δ 174.2, 174.0, 173.9, 85.9, 82.8, 82.5, 80.3, 75.3, 55.8, 52.2, 50.8, 49.6, 46.2, 39.6, 39.0, 38.5, 38.0, 37.0, 34.4, 31.0, 28.9, 28.3, 28.2, 28.0, 28.0, 26.9, 25.8, 23.6, 22.9, 21.7, 21.6, 18.1, 17.4, 16.5, 16.0, 15.6, 9.3 (2C), 9.0. HR-ESI-MS *m/z* for $C_{39}H_{65}O_7$ $[M+H]^+$: calcd., 645.4652; found: 645.4672.

*3.1.2.3. (20S, 24R)-epoxy-3β, 12β, 25-O-tributyryl-dammarane (**3c**).* Transparent oil, yield 24.6 %, ^{1}H NMR (600 MHz, $CDCl_3$) δ 4.86−4.82 (m, 1 H), 4.48−4.46 (m, 1 H), 3.86 (t, *J* =12.0 Hz, 1 H), 2.26−2.14 (m, 6 H), 2.02−1.97 (m, 1 H), 1.91−1.67 (m, 7 H), 1.66−1.43 (m, 17 H), 1.41 (s, 3 H), 1.39 (s, 3 H), 1.30−1.21 (m, 3 H), 1.13 (s, 3 H), 0.96 (s, 3 H), 0.93−0.92 (m, 6 H), 0.91 (s, 2 H), 0.90 (s, 3 H), 0.89 (s, 1 H), 0.84 (s, 3 H), 0.82 (s, 6 H). ^{13}C NMR (150 MHz, $CDCl_3$) δ 173.4, 173.1 (2C), 85.9, 82.8, 82.5, 80.2, 75.2, 55.8, 52.2, 50.8, 49.6, 46.2, 39.6, 39.1, 38.5, 37.9, 37.6, 37.0, 36.8, 36.7, 34.4, 31.0, 28.3, 28.0, 26.9, 25.8, 23.6, 22.9, 21.7 (2C), 18.7, 18.6, 18.3, 18.1, 17.4, 16.6, 16.0, 15.6, 13.7 (2C), 13.6. HR-ESI-MS *m/z* for $C_{42}H_{71}O_7$ $[M+H]^+$: calcd., 687.5122; found: 687.5146.

*3.1.2.4. (20S, 24R)-epoxy-3β, 12β, 25-O-trivaleryl-dammarane (**3d**).* Transparent oil, yield 17.1 %, ^{1}H NMR (600 MHz, $CDCl_3$) δ 4.89−4.85 (m, 1 H), 4.52−4.49 (m, 1 H), 3.90 (t, *J* =6.0 Hz, 1 H), 2.32−2.20 (m, 6 H), 2.06 (s, 1 H), 2.04−2.01 (m, 1 H), 1.94−1.73 (m, 6 H), 1.70−1.47 (m, 16 H), 1.44 (s, 3 H),1.43 (s, 3 H), 1.40−1.26 (m, 10 H), 1.17 (s, 3 H), 1.00 (s, 3 H), 0.95−0.91 (m, 12 H), 0.88 (s, 3 H), 0.86 (s, 6 H). ^{13}C NMR (150 MHz, $CDCl_3$) δ 173.5, 173.3, 173.2, 85.9, 82.7, 82.5, 80.2, 75.2, 55.82, 52.2, 50.8, 49.6, 46.2, 39.6, 39.1, 38.5, 37.9, 37.0, 35.4, 34.6,

34.5, 34.4, 31.0, 28.3, 28.0, 27.3, 27.2, 26.9 (2C), 25.8, 23.6, 22.9, 22.3 (2C), 22.2, 21.7 (2C), 18.1, 17.4, 16.6, 16.0, 15.6, 13.8, 13.7, 13.7. HR-ESI-MS *m/z* for $C_{45}H_{77}O_7$ $[M+H]^+$: calcd., 729.5591; found: 729.5566.

3.1.2.5. (20S, 24R)-epoxy-3β, 12β, 25-O-trihexanoyl-dammarane ***(3e)***. Transparent oil, yield 19.6 %, ^{1}H NMR (600 MHz, $CDCl_3$) δ 4.90−4.85 (m, 1 H), 4.52−4.49 (m, 1 H), 3.91 (t, J =6.0 Hz, 1 H), 2.32−2.20 (m, 6 H), 2.06−2.01 (m, 1 H), 1.95−1.73 (m, 7 H), 1.70−1.48 (m, 17 H), 1.44 (s, 3 H),1.43 (s, 3 H), 1.36−1.25 (m, 15 H), 1.17 (s, 3 H), 1.01 (s, 3 H), 0.95 (s, 3 H), 0.93−0.90 (m, 9 H), 0.88 (s, 3 H), 0.87 (s, 6 H). ^{13}C NMR (150 MHz, $CDCl_3$) δ 173.6, 173.3 (2C), 85.9, 82.7, 82.4, 80.2, 75.2, 55.8, 52.2, 50.8, 49.6, 46.2, 39.6, 39.1, 38.5, 37.9, 37.0, 35.7, 34.9, 34.8, 34.4, 32.7 (2C), 32.6, 31.3 (2C), 31.2, 31.0, 28.3, 28.0, 26.9, 25.8, 24.8, 24.5, 23.6, 22.9, 22.3, 21.7 (2C), 18.1, 17.4, 16.6, 16.0, 15.6, 13.9, 13.9, 13.9. HR-ESI-MS *m/z* for $C_{48}H_{83}O_7$ $[M+H]^+$: calcd., 771.6061; found: 771.6031.

3.1.2.6. (20S, 24R)-epoxy-3β, 12β, 25-O-triheptanoyl-dammarane ***(3f)***. Transparent oil, yield 22.2 %, ^{1}H NMR (600 MHz, $CDCl_3$) δ 4.90−4.85 (m, 1 H), 4.52−4.49 (m, 1 H), 3.92−3.89 (m, 1 H), 2.33−2.20 (m, 6 H), 2.06−2.01 (m, 1 H), 1.94−1.73 (m, 6 H), 1.70−1.47 (m, 16 H), 1.44 (s, 3 H), 1.43 (s, 3 H), 1.31−1.26 (m, 20 H), 1.17 (s, 3 H), 1.14−1.01 (m, 3 H), 1.00 (s, 3 H), 0.95 (s, 3 H), 0.91−0.89 (m, 9 H), 0.88 (s, 3 H), 0.86 (s, 6 H). ^{13}C NMR (150 MHz, $CDCl_3$) δ 173.5, 173.3, 173.2, 85.9, 82.7, 82.4, 80.2, 75.2, 55.8, 52.2, 50.8, 49.6, 46.2, 39.6, 39.1, 38.5, 37.9, 37.0, 35.7, 34.9, 34.8, 34.4, 31.6, 31.5, 31.5, 31.0, 28.8 (2C), 28.8, 28.3, 28.0, 26.9, 25.8, 25.2, 25.1, 24.8, 23.6, 22.9, 22.5, 22.5, 22.4, 21.7 (2C), 18.1, 17.4, 16.6, 16.0, 15.6, 14.0 (2C), 13.9. HR-ESI-MS *m/z* for $C_{51}H_{89}O_7$ $[M+H]^+$: calcd., 813.6530; found: 813.6500.

3.1.2.7. (20S, 24R)-epoxy-3β, 12β, 25-O-trioctanoyl-dammarane ***(3g)***. Transparent oil, yield 12.9 %, ^{1}H NMR (600 MHz, $CDCl_3$) δ 4.90−4.85 (m, 1 H), 4.52−4.49 (m, 1 H), 3.92−3.89 (m, 1 H), 2.31−2.20 (m, 6 H), 2.07−2.01 (m, 1 H), 1.95−1.73 (m, 6 H), 1.70−1.47 (m, 17 H), 1.44 (s, 3 H),1.43 (s, 3 H), 1.31−1.27 (m, 30 H), 1.17 (s, 3 H), 1.00 (s, 3 H), 0.94 (s, 3 H), 0.90−0.89 (m, 9 H), 0.88 (s, 3 H), 0.86 (s, 6 H). ^{13}C NMR (150 MHz, $CDCl_3$) δ 173.6, 173.3, 173.3, 85.9, 82.7, 82.4, 80.2, 75.2, 55.8, 52.2, 50.8, 49.6, 46.2, 39.6, 39.1, 38.5, 37.9, 37.0, 35.7, 34.9, 34.8, 34.4, 32.0, 31.8, 31.7, 31.0, 29.1 (2C), 29.0, 28.9 (3C), 28.3, 28.0, 26.9, 25.8, 25.1 (2C), 24.8, 23.6, 22.8, 22.6 (2C), 22.5, 21.7 (2C), 18.1, 17.4, 16.6, 16.0, 15.6, 14.1, 14.0 (2C). HR-ESI-MS *m/z* for $C_{54}H_{95}O_7$ $[M+H]^+$: calcd., 855.7000; found: 855.7030.

3.1.2.8. (20S, 24R)-epoxy-3β, 12β-O-dibutyryl-dammarane-25-ol ***(4a)***. White solid, yield 32.5 %, ^{1}H NMR (600 MHz, $CDCl_3$) δ 5.57 (s, 1 H), 4.91−4.86 (m, 1 H), 4.53–4.50 (m, 1 H), 3.68−3.65 (m, 1 H), 2.31−2.28 (m, 2 H), 2.27−2.23 (m, 2 H), 2.06−2.01 (m, 1 H), 1.96−1.91 (m, 1 H), 1.90−1.79 (m, 5 H), 1.78−1.62 (m, 11 H), 1.59−1.43 (m, 6 H), 1.33−1.31 (m, 1 H), 1.21 (s, 3 H), 1.20 (s, 3 H), 1.12 (s, 3 H), 1.09−1.07 (m, 1 H), 1.01 (s, 3 H), 0.99−0.95 (m, 9 H), 0.89 (s, 3 H), 0.87 (s, 6 H). ^{13}C NMR (150 MHz, $CDCl_3$) δ 173.4, 173.2, 85.7, 83.4, 80.2, 75.1, 71.0, 55.8, 52.1, 50.6, 49.6, 46.3, 39.6, 39.0, 38.5, 37.9, 37.0, 36.8, 36.7, 34.4, 31.1, 28.4, 28.0, 27.5, 26.8, 26.0, 24.2, 23.6, 22.3, 18.6, 18.3, 18.1, 17.5, 16.6, 16.1, 15.6, 13.7, 13.7. HR-ESI-MS *m/z* for $C_{38}H_{65}O_6$ $[M+H]^+$: calcd., 617.4703; found: 617.4722.

3.1.2.9. (20S, 24R)-epoxy-3β, 12β-O-divaleryl-dammarane-25-ol ***(4b)***. Transparent oil, yield 26.6 %, ^{1}H NMR (600 MHz, $CDCl_3$) δ 5.58 (s. 1 H), 4.90−4.85 (m, 1 H), 4.52−4.50 (m, 1 H), 3.68−3.66 (m, 1 H), 2.33−2.30 (m, 2 H), 2.28−2.25 (m, 3 H), 2.06−2.01 (m, 1 H), 1.94−1.92 (m, 1 H), 1.89−1.78 (m, 3 H), 1.76−1.43 (m, 17 H), 1.40−1.31 (m, 5 H), 1.27−1.25 (m, 2 H), 1.21 (s, 3 H), 1.20 (s, 3 H), 1.12 (s, 3 H), 1.01 (s, 3 H), 0.96 (s, 3 H), 0.95−0.92 (m, 6 H), 0.89 (s, 3 H), 0.87 (s, 6 H). ^{13}C NMR (150 MHz, $CDCl_3$) δ 173.5, 173.3, 85.7, 83.4, 80.2, 75.1, 71.0, 55.8, 52.1, 50.6, 49.6, 46.3, 39.6, 39.0, 38.5, 37.9, 37.0, 34.6, 34.5, 34.4, 31.2, 28.4, 28.0, 27.5, 27.2, 26.9, 26.8 (2C), 26.0, 24.2, 23.6, 22.3 (2C), 18.1, 17.5, 16.6, 16.1, 15.6, 13.8, 13.7. HR-ESI-MS *m/z* for $C_{40}H_{69}O_6$ $[M+H]^+$: calcd., 645.5016; found: 645.5040.

3.1.2.10. (20S, 24R)-epoxy-3β, 12β-O-dihexanoyl-dammarane-25-ol ***(4c)***. Transparent oil, yield 35.1 %, ^{1}H NMR (600 MHz, $CDCl_3$) δ 5.50 (s, 1 H), 4.89−4.85 (m, 1 H), 4.52−4.49 (m, 1 H), 3.68−3.65 (m, 1 H), 2.34−2.21 (m, 5 H), 2.06−2.01 (m, 1 H), 1.95−1.90 (m, 1 H), 1.89−1.78 (m, 3 H), 1.77−1.70 (m, 2 H), 1.69−1.61 (m, 8 H), 1.60−1.55 (m, 3 H), 1.53−1.45 (m, 3 H), 1.38−1.30 (m, 9 H), 1.27 (s, 3 H), 1.20 (s, 3 H),1.19 (s, 3 H), 1.11 (s, 3 H), 1.01 (s, 3 H), 0.95 (s, 3 H), 0.92−0.90 (m, 6 H), 0.88 (s, 3 H), 0.86 (s, 6 H). ^{13}C NMR (150 MHz, $CDCl_3$) δ 173.5, 173.3, 85.7, 83.4, 80.2, 75.1, 71.0, 55.8, 52.1, 50.6, 49.6, 46.3, 39.6, 39.0, 38.5, 37.9, 37.0, 34.8, 34.8, 34.4, 31.3, 31.1, 29.7, 28.4, 28.0, 27.5, 26.8, 26.0, 24.8, 24.5, 24.2, 23.6 (2C), 22.3, 22.3, 18.1, 17.5, 16.6, 16.0, 15.6, 13.9, 13.9. HR-ESI-MS *m/z* for $C_{42}H_{73}O_6$ $[M+H]^+$: calcd., 673.5329; found: 673.5303.

3.1.2.11. (20S, 24R)-epoxy-3β, 12β-O-diheptanoyl-dammarane-25-ol ***(4d)***. Transparent oil, yield 37.4 %, ^{1}H NMR (600 MHz, $CDCl_3$) δ 5.52 (s, 1 H), 4.90−4.85 (m, 1 H), 4.52−4.49 (m, 1 H), 3.68−3.65 (m, 1 H), 2.32−2.21 (m, 5 H), 2.06−2.01 (m, 1 H), 1.95−1.90 (m, 1 H), 1.89−1.78 (m, 4 H), 1.76−1.55 (m, 14 H), 1.53−1.43 (m, 3 H), 1.36−1.26 (m, 14 H), 1.20 (s, 3 H), 1.20 (s, 3 H), 1.112 (s, 3 H), 1.01 (s, 3 H), 0.95 (s, 3 H), 0.91−0.90 (m, 6 H), 0.89 (s, 3 H), 0.87 (s, 6 H). ^{13}C NMR (150 MHz, $CDCl_3$) δ 173.6, 173.4, 85.7, 83.4, 80.2, 75.1, 71.0, 55.8, 52.1, 50.6, 49.6, 46.3, 39.6, 39.0, 38.5, 37.9, 37.0, 34.9, 34.8, 34.4, 31.5, 31.1, 31.0, 29.0, 28.8, 28.4, 28.0, 27.5, 26.8, 26.0, 25.1 (2C), 24.8, 24.2, 23.6, 22.5, 22.3, 18.1, 17.5, 16.6, 16.0, 15.6, 14.0 (2C). HR-ESI-MS *m/z* for $C_{44}H_{77}O_6$ $[M+H]^+$: calcd., 701.5642; found: 701.5618.

3.1.2.12. (20S, 24R)-epoxy-3β, 12β-O-dicaprylyl-dammarane-25-ol ***(4e)***. Transparent oil, yield 32.6 %, ^{1}H NMR (600 MHz, $CDCl_3$) δ 5.51 (s, 1 H), 4.87−4.83 (m, 1 H), 4.49−4.47 (m, 1 H), 3.64 (t, J =6.0 Hz, 1 H), 2.29−2.21 (m, 5 H), 2.03−1.98 (m, 1 H), 1.91−1.88 (m, 1 H), 1.84−1.75 (m, 3 H), 1.73−1.41 (m, 17 H), 1.30−1.27 (m, 18 H), 1.18 (s, 3 H), 1.17 (s, 3 H), 1.13 (d, J =12.0 Hz, 1 H), 1.09 (s, 3 H), 0.98 (s, 3 H), 0.93 (s, 3 H), 0.87 (t, J =12.0 Hz, 9 H), 0.84 (s, 6 H). ^{13}C NMR (150 MHz, $CDCl_3$) δ 173.6, 173.4, 85.7, 83.4, 80.2, 75.1, 71.0, 55.8, 52.1, 50.6, 49.6, 46.3, 39.6, 39.0, 38.5, 37.9, 37.0, 34.9, 34.8, 34.4, 31.7, 31.1, 30.1, 29.2, 29.1, 29.1, 28.9, 28.4, 28.0, 27.5, 26.8, 26.0, 25.1, 24.8, 24.2, 23.6, 22.6, 22.2, 18.1, 17.5, 16.6, 16.0, 15.6, 14.1, 14.0. HR-ESI-MS *m/z* for $C_{46}H_{81}O_6$ $[M+H]^+$: calcd., 729.5955; found: 729.5930.

3.1.3. General Procedure for the Preparation of ***5a-5f*** *and* ***6a-6g***

KOH (4.71 mmol) was added to the mixture of compound **3a-3g** or **4a-4e** (1.81 mmol) in EtOH (20 mL), and stirred for 24 h at 25 ℃. The mixture was diluted with water to pH 7.0, and then extracted with ethyl acetate (3 × 10 mL). The organic layer was washed by water (3 × 10 mL) and saturated brine (3 × 10 mL) successively, dried over anhydrous Na_2SO_4 and evaporated. The residue was purified by column chromatography (*n*-hexane: ethyl acetate) to afford compounds **5a-5f** and **6a-6g.**

3.1.3.1. (20S, 24R)-epoxy-12β, 25-O-diacetyl-dammarane-3β-ol ***(5a)***. White solid, yield 4.3 %, ^{1}H NMR (600 MHz, $CDCl_3$) δ 5.57 (s, 1 H), 4.88−4.83 (m, 1 H), 3.91 (t, J =6.0 Hz, 1 H), 3.23−3.21 (m, 1 H), 2.03 (s, 3 H), 1.98 (s, 3 H), 1.96−1.88 (m, 3 H), 1.86−1.78 (m, 3 H), 1.72−1.61 (m, 6 H), 1.60−1.52 (m, 4 H), 1.49−1.47 (m, 2 H), 1.45 (s, 3 H), 1.45 (s, 3 H), 1.28 (s, 3 H), 1.18 (s, 3 H), 1.06−1.04 (m, 1 H), 1.01 (s, 3 H), 1.00 (s, 3 H), 0.95 (s, 3 H), 0.87 (s, 3 H), 0.80 (s, 3 H). ^{13}C NMR (150 MHz, $CDCl_3$) δ 170.6, 170.4, 86.0, 83.2, 82.5, 78.8, 75.6, 55.8, 52.2, 50.8, 49.8, 46.2, 39.6, 39.0 (2C), 38.8, 37.1, 34.5, 31.1, 28.4, 28.0, 27.2, 27.0, 25.9, 22.7, 22.5, 21.9, 21.8, 21.6, 18.2, 17.5, 16.0, 15.6, 15.4. HR-ESI-MS *m/z* for $C_{34}H_{57}O_6$ $[M+H]^+$: calcd., 561.4077; found:

561.4059.

*3.1.3.2. (20S, 24R)-epoxy-12β, 25-O-dipropionyl-dammarane-3β-ol (**5b**).* Transparent oil, yield 7.6 %, ^{1}H NMR (600 MHz, $CDCl_3$) δ 5.54 (s, 1 H), 4.90−4.85 (m, 1 H), 3.91 (t, J =6.0 Hz, 1 H), 3.23−3.21 (m, 1 H), 2.31−2.23 (m, 4 H), 2.07−2.01 (m, 1 H), 1.95−1.74 (m, 7 H), 1.69−1.47 (m, 11 H), 1.45 (s, 6 H), 1.28 (s, 3 H), 1.18 (s, 3 H), 1.14 (t, J =6.0 Hz, 3 H), 1.11 (t, J =6.0 Hz, 3 H), 1.01 (s, 3 H), 1.00 (s, 3 H), 0.95 (s, 3 H), 0.87 (s, 3 H), 0.79 (s, 3 H). ^{13}C NMR (150 MHz, $CDCl_3$) δ 174.0, 173.8, 86.0, 82.8, 82.4, 78.8, 75.4, 55.8, 52.2, 50.8, 49.7, 46.2, 39.6, 39.0, 38.9, 38.8, 37.1, 34.5, 31.0, 28.9, 28.4, 28.2, 28.0, 27.2, 26.9, 25.9, 22.9, 21.7, 21.6, 18.2, 17.5, 16.0, 15.6, 15.4, 9.3, 9.0. HR-ESI-MS m/z for $C_{36}H_{61}O_6$ $[M+H]^+$: calcd., 589.4390; found: 589.4369.

*3.1.3.3. (20S, 24R)-epoxy-12β, 25-O-dibutyryl-dammarane-3β-ol (**5c**).* Transparent oil, yield 21.0 %, ^{1}H NMR (600 MHz, $CDCl_3$) δ 5.56 (s, 1 H), 4.90−4.85 (m, 1 H), 3.91 (t, J =6.0 Hz, 1 H), 3.23−3.21 (m, 1 H), 2.27−2.19 (m, 4 H), 2.06−2.01 (m, 1 H), 1.95−1.74 (m, 7 H), 1.68−1.61 (m, 8 H), 1.59−1.52 (m, 4 H), 1.50−1.46 (m, 2 H), 1.45 (s, 3 H), 1.44 (s, 3 H), 1.33−1.27 (m, 2 H), 1.18 (s, 3 H), 1.07−1.03 (m, 2 H), 1.01 (s, 3 H), 1.00 (s, 3 H), 0.98−0.96 (m, 5 H), 0.95 (s, 3 H), 0.94 (s, 1 H), 0.86 (s, 3 H), 0.80 (s, 3 H). ^{13}C NMR (150 MHz, $CDCl_3$) δ 173.2, 173.0, 85.9, 82.8, 82.4, 78.8, 75.3, 55.8, 52.2, 50.8, 49.7, 46.2, 39.6, 39.1, 38.9, 38.8, 37.7, 37.1, 36.8, 34.5, 31.0, 28.4, 28.0, 27.2, 26.9, 25.7, 22.9, 21.7, 21.7, 18.7, 18.3, 18.2, 17.5, 16.0, 15.6, 15.4, 13.7, 13.6. HR-ESI-MS m/z for $C_{38}H_{65}O_6$ $[M+H]^+$: calcd., 617.4703; found: 617.4680.

*3.1.3.4. (20S, 24R)-epoxy-12β, 25-O-divaleryl-dammarane-3β-ol (**5d**).* Transparent oil, yield 9.5 %, ^{1}H NMR (600 MHz, $CDCl_3$) δ 5.54 (s, 1 H), 4.89−4.85 (m, 1 H), 3.91 (t, J =6.0 Hz, 1 H), 3.24−3.21 (m, 1 H), 2.28−2.19 (m, 4 H), 2.05−2.01 (m, 1 H), 1.95−1.74 (m, 7 H), 1.69−1.55 (m, 13 H), 1.45 (s, 3 H), 1.44 (s, 3 H), 1.38−1.33 (m, 5 H), 1.30−1.27 (m, 1 H), 1.18 (s, 3 H), 1.07−1.03 (m, 2 H), 1.01 (s, 3 H), 1.00 (s, 3 H), 0.95 (s, 3 H), 0.94−0.92 (m, 7 H), 0.86 (s, 3 H), 0.80 (s, 3 H). ^{13}C NMR (150 MHz, $CDCl_3$) δ 173.4, 173.2, 85.9, 82.8, 82.4, 78.8, 75.3, 55.8, 52.2, 50.8, 49.7, 46.2, 39.6, 39.1, 38.9, 38.8, 37.1, 35.5, 34.6, 34.5, 31.0, 28.3, 28.0, 27.3, 27.3, 27.2, 26.9, 25.9, 22.9, 22.3, 22.2, 21.7, 21.7, 18.2, 17.5, 16.0, 15.6, 15.6, 13.8, 13.7. HR-ESI-MS m/z for $C_{40}H_{69}O_6$ $[M+H]^+$: calcd., 645.5016; found: 645.5038.

*3.1.3.5. (20S, 24R)-epoxy-12β, 25-O-dihexanoyl-dammarane-3β-ol (**5e**).* Transparent oil, yield 11.9 %, ^{1}H NMR (600 MHz, $CDCl_3$) δ 5.56 (s, 1 H), 4.89−4.85 (m, 1 H), 3.91 (t, J =6.0 Hz, 1 H), 3.28−3.20 (m, 1 H), 2.28−2.20 (m, 4 H), 2.05−2.01 (m, 1 H), 1.95−1.74 (m, 6 H), 1.70−1.55 (m, 14 H), 1.50−1.48 (m, 2 H), 1.45 (s, 3 H), 1.44 (s, 3 H), 1.36−1.30 (m, 9 H), 1.29−1.27 (m, 2 H), 1.18 (s, 3 H), 1.01 (s, 3 H), 1.00 (s, 3 H), 0.95 (s, 3 H), 0.94−0.92 (m, 3 H), 0.91−0.99 (m, 3 H), 0.87 (s, 3 H), 0.80 (s, 3 H). ^{13}C NMR (150 MHz, $CDCl_3$) δ 173.4, 173.3, 85.9, 82.8, 82.4, 78.8, 75.3, 55.8, 52.2, 50.8, 49.7, 46.2, 39.6, 39.1, 38.9, 38.8, 37.1, 35.7, 34.9, 34.5, 31.4, 31.4, 31.3 (2C), 31.0, 28.3, 28.0, 27.2, 26.9, 25.9, 24.8, 24.5, 22.9, 21.7, 21.6, 18.2, 17.5, 16.0, 15.6, 15.4, 13.9 (2C). HR-ESI-MS m/z for $C_{42}H_{73}O_6$ $[M+H]^+$: calcd., 673.5329; found: 673.5351.

*3.1.3.6. (20S, 24R)-epoxy-12β, 25-O-diheptanoyl-dammarane-3β-ol (**5f**).* Transparent oil, yield 21.8 %, ^{1}H NMR (600 MHz, $CDCl_3$) δ 5.53 (s, 1 H), 4.89−4.85 (m, 1 H), 3.91 (t, J =6.0 Hz, 1 H), 3.24−3.21 (m, 1 H), 2.29−2.20 (m, 4 H), 2.05−2.01 (m, 1 H), 1.95−1.74 (m, 6 H), 1.71−1.53 (m, 12 H), 1.52−1.48 (m, 3 H), 1.45 (s, 3 H), 1.44 (s, 3 H), 1.33−1.28 (m, 14 H), 1.18 (s, 3 H), 1.07−1.04 (m, 2 H), 1.01 (s, 3 H), 1.00 (s, 3 H), 0.95 (s, 3 H), 0.92−0.89 (m, 6 H), 0.86 (s, 3 H), 0.80 (s, 3 H). ^{13}C NMR (150 MHz, $CDCl_3$) δ 173.4, 173.2, 85.9, 82.8, 82.4, 78.8, 75.3, 55.8, 52.2, 50.8, 49.7, 46.2, 39.6, 39.1, 38.9, 38.8, 37.1, 35.7, 34.9, 34.5, 31.5, 31.5, 31.0, 28.8, 28.8, 28.4, 28.0, 27.2, 26.9, 25.9, 25.1, 24.8, 22.9, 22.5 (2C), 21.7, 21.6, 18.2, 17.5, 16.0, 15.6, 15.4, 14.0, 14.0. HR-ESI-MS m/z for $C_{44}H_{77}O_6$ $[M+H]^+$: calcd., 701.5642; found: 701.5618.

*3.1.3.7. (20S, 24R)-epoxy-12β-O-acetyl-dammarane-3β, 25-diol (**6a**).* White solid, yield 10.4 %, ^{1}H NMR (600 MHz, $CDCl_3$) δ 5.52 (s, 1 H), 4.87−4.83 (m, 1 H), 4.56 (s, 1 H), 3.68−3.66 (m, 1 H), 3.23−3.21 (m, 1 H), 2.03 (s, 3 H), 1.97−1.92 (m, 1 H), 1.89−1.69 (m, 8 H), 1.67−1.63 (m, 3 H), 1.61−1.54 (m, 3 H), 1.52−1.45 (m, 3 H), 1.34−1.27 (m, 2 H), 1.21 (s, 3 H), 1.20 (s, 3 H), 1.12 (s, 3 H), 1.09−1.04 (m, 2 H), 1.01 (s, 3 H), 1.00 (s, 3 H), 0.96 (s, 3 H), 0.87 (s, 3 H), 0.79 (s, 3 H). ^{13}C NMR (150 MHz, $CDCl_3$) δ 170.6, 85.7, 83.4, 78.8, 75.5, 71.0, 55.8, 52.2, 50.5, 49.8,46.3, 39.6, 38.9, 38.9, 38.8, 37.1, 34.5, 31.2, 28.4, 28.0, 27.6, 27.2, 26.8, 26.1, 24.2, 22.3, 21.9, 18.2, 17.6, 16.0, 15.5, 15.3. HR-ESI-MS m/z for $C_{32}H_{55}O_5$ $[M+H]^+$: calcd., 519.3971; found: 519.3955.

*3.1.3.8. (20S, 24R)-epoxy-12β-O-propionyl-dammarane-3β, 25-diol (**6b**).* White solid, yield 25.7 %, ^{1}H NMR (600 MHz, $CDCl_3$) δ 5.54 (s, 1 H), 4.89−4.85 (m, 1 H), 4.52 (s, 1 H), 3.68−3.65 (m, 1 H), 3.23−3.21 (m, 1 H), 2.31−2.27 (m, 2 H), 2.05−2.01 (m, 1 H), 1.95−1.92 (m, 1 H), 1.87−1.82 (m, 2 H), 1.82−1.70 (m, 5 H), 1.69−1.62 (m, 4 H), 1.61−1.54 (m, 3 H), 1.52−1.45 (m, 3 H), 1.34−1.31 (m, 1 H), 1.21 (s, 3 H), 1.20 (s, 3 H), 1.14 (t, J =6.0 Hz, 3 H), 1.12 (s, 3 H), 1.09−1.03 (m, 2 H), 1.01 (s, 3 H), 1.00 (s, 3 H), 0.96 (s, 3 H), 0.87 (s, 3 H), 0.79 (s, 3 H). ^{13}C NMR (150 MHz, $CDCl_3$) δ 174.0, 85.7, 83.4, 78.8, 75.3, 71.0, 55.8, 52.2, 50.5, 49.8, 46.3, 39.6, 38.9 (2C), 38.8, 37.1, 34.5, 31.2, 28.4, 28.2, 28.0, 27.5, 27.2, 26.8, 26.0, 24.2, 22.3, 18.2, 17.6, 16.0, 15.6, 15.3, 9.0. HR-ESI-MS m/z for $C_{33}H_{57}O_5$ $[M+H]^+$: calcd., 533.4128; found: 533.4145.

*3.1.3.9. (20S, 24R)-epoxy-12β-O-butyryl-dammarane-3β, 25-diol (**6c**).* White solid, yield 12.6 %, ^{1}H NMR (600 MHz, $CDCl_3$) δ 5.53 (s, 1 H), 4.90−4.85 (m, 1 H), 4.54 (s, 1 H), 3.68−3.66 (m, 1 H), 3.24−3.21 (m, 1 H), 2.29−2.20 (m, 2 H), 2.05−2.01 (m, 1 H), 1.95−1.92 (m, 1 H), 1.89−1.79 (m, 3 H), 1.78−1.63 (m, 10 H), 1.61−1.56 (m, 3 H), 1.54−1.45 (m, 3 H), 1.34−1.31 (m, 1 H), 1.21 (s, 3 H), 1.20 (s, 3 H), 1.12 (s, 3 H), 1.09−1.04 (m, 2 H), 1.01 (s, 3 H), 1.00 (s, 3 H), 0.98 (s, 1 H), 0.97 (s, 1 H), 0.96 (s, 3 H), 0.95 (s, 1 H), 0.86 (s, 3 H), 0.80 (s, 3 H). ^{13}C NMR (150 MHz, $CDCl_3$) δ 173.2, 85.7, 83.4, 78.8, 75.2, 71.0, 1.00, 55.8, 52.2, 50.6, 49.8, 46.3, 39.6, 39.0, 38.9, 38.8, 37.1, 36.8, 34.5, 31.2, 28.4, 28.0, 27.5, 27.2, 26.8, 26.0, 24.2, 22.3, 18.3, 18.2, 17.6, 16.0, 15.6, 15.4, 13.7. HR-ESI-MS m/z for $C_{34}H_{59}O_5$ $[M+H]^+$: calcd., 547.4284; found: 547.4263.

*3.1.3.10. (20S, 24R)-epoxy-12β-O-valeryl-dammarane-3β, 25-diol (**6d**).* White solid, yield 42.5 %, ^{1}H NMR (600 MHz, $CDCl_3$) δ 5.57 (s, 1 H), 4.89−4.84 (m, 1 H), 4.56 (s, 1 H), 3.68−3.66 (m, 1 H), 3.24−3.21 (m, 1 H), 2.31−2.22 (m, 2 H), 2.05−2.00 (m, 1 H), 1.95−1.92 (m, 1 H), 1.89−1.79 (m, 3 H), 1.78−1.69 (m, 4 H), 1.68−1.54 (m, 9 H), 1.52−1.45 (m, 3 H), 1.41−1.31 (m, 3 H), 1.21 (s, 3 H), 1.20 (s, 3 H), 1.17−1.15 (m, 2 H), 1.12 (s, 3 H), 1.09−1.04 (m, 2 H), 1.01 (s, 3 H), 1.00 (s, 3 H), 0.96 (s, 3 H), 0.94 (t, J =6.0 Hz, 3 H), 0.87 (s, 3 H), 0.80 (s, 3 H). ^{13}C NMR (150 MHz, $CDCl_3$) δ 173.4, 85.7, 83.4, 78.8, 75.2, 71.0, 55.8, 52.2, 50.6, 49.8, 46.3, 39.6, 39.0, 38.9, 38.8, 37.1, 34.6, 34.5, 31.2, 28.4, 28.0, 27.5, 27.2, 26.9, 26.8, 26.0, 24.2, 22.3 (2C), 18.2, 17.6, 16.0, 15.6, 15.4, 13.8. HR-ESI-MS m/z for $C_{35}H_{61}O_5$ $[M+H]^+$: calcd., 561.4441; found: 561.4422.

*3.1.3.11. (20S, 24R)-epoxy-12β-O-hexanoyl-dammarane-3β, 25-diol (**6e**).* White solid, yield 46.1 %, ^{1}H NMR (600 MHz, $CDCl_3$) δ 5.59 (s, 1 H), 4.89−4.84 (m, 1 H), 4.59 (s, 1 H), 3.68−3.66 (m, 1 H), 3.24−3.21 (m, 1 H), 2.30−2.21 (m, 2 H), 2.05−2.01 (m, 1 H), 1.95−1.92 (m, 1 H), 1.89−1.79 (m, 3 H), 1.77−1.62 (m, 10 H), 1.60−1.54 (m, 3 H), 1.52−1.43 (m, 3 H), 1.38−1.28 (m, 6 H), 1.21 (s, 3 H), 1.20 (s, 3 H), 1.18−1.15 (m, 1 H), 1.01 (s, 3 H), 1.00 (s, 3 H), 0.96 (s, 3 H), 0.92 (t, J

=6.0 Hz, 3 H), 0.87 (s, 3 H), 0.80 (s, 3 H). ^{13}C NMR (150 MHz, $CDCl_3$) δ 173.4, 85.7, 83.4, 78.8, 75.2, 71.0, 55.8, 52.2, 50.6, 49.8, 46.3, 39.6, 39.0, 38.9, 38.8, 37.1, 34.8, 34.5, 31.3, 31.2 (2C), 28.4, 28.0, 27.5, 27.2, 26.8, 26.0, 24.5, 24.2, 22.2, 18.2, 17.6, 16.0, 15.6, 15.3, 13.9. HR-ESI-MS *m/z* for $C_{36}H_{63}O_5$ $[M+H]^+$: calcd., 575.4597; found: 575.4579.

*3.1.3.12. (20S, 24R)-epoxy-12β-O-heptanoyl-dammarane-3β, 25-diol (**6f**).* White solid, yield 37.8 %, ^{1}H NMR (600 MHz, $CDCl_3$) δ 5.59 (s, 1 H), 4.89−4.84 (m, 1 H), 4.59 (s, 1 H), 3.68−3.66 (m, 1 H), 3.23−3.21 (m, 1 H), 2.30−2.21 (m, 2 H), 2.05−2.00 (m, 1 H), 1.95−1.92 (m, 1 H), 1.89−1.70 (m, 7 H), 1.69−1.54 (m, 9 H), 1.52−1.43 (m, 3 H), 1.35−1.28 (m, 8 H), 1.21 (s, 3 H), 1.20 (s, 3 H), 1.17−1.15 (m, 1 H), 1.12 (s, 3 H), 1.09−1.04 (m, 2 H), 1.01 (s, 3 H), 1.00 (s, 3 H), 0.96 (s, 3 H), 0.91 (t, *J* =6.0 Hz, 3 H), 0.86 (s, 3 H), 0.79 (s, 3 H). ^{13}C NMR (150 MHz, $CDCl_3$) δ 173.4, 85.7, 83.4, 78.8, 75.2, 71.0, 55.8, 52.2, 50.6, 49.8, 46.3, 39.6, 39.0, 38.9, 38.8, 37.1, 34.9, 34.5, 31.5, 31.2, 28.8, 28.4, 28.0, 27.5, 27.2, 26.8, 26.0, 24.8, 24.2, 22.5, 22.2, 18.2, 17.6, 16.0, 15.6, 15.3, 14.0. HR-ESI-MS *m/z* for $C_{37}H_{65}O_5$ $[M+H]^+$: calcd., 589.4754; found: 589.4733.

*3.1.3.13. (20S, 24R)-epoxy-12β-O-octanoyl-dammarane-3β, 25-diol (**6g**).* White solid, yield 28.7 %, ^{1}H NMR (600 MHz, $CDCl_3$) δ 5.57 (s, 1 H), 4.88−4.84 (m, 1 H), 4.55 (s, 1 H), 3.68−3.66 (m, 1 H), 3.23−3.21 (m, 1 H), 2.27−2.24 (m, 2 H), 2.05−2.00 (m, 1 H), 1.95−1.91 (m, 1 H), 1.89−1.78 (m, 3 H), 1.77−1.54 (m, 14 H), 1.52−1.43 (m, 3 H), 1.33−1.27 (m, 10 H), 1.21 (s, 3 H), 1.20 (s, 3 H), 1.12 (s, 3 H), 1.01 (s, 3 H), 1.00 (s, 3 H), 0.96 (s, 3 H), 0.90 (t, *J* =6.0 Hz, 3 H), 0.86 (s, 3 H), 0.79 (s, 3 H). ^{13}C NMR (150 MHz, $CDCl_3$) δ 173.4, 85.8, 83.4, 78.8, 75.2, 71.0, 55.7, 52.2, 50.6, 49.8, 46.3, 39.6, 39.0, 38.9, 38.8, 37.1, 34.9, 34.5, 31.7, 31.2, 29.1, 28.9, 28.4, 28.0, 27.5, 27.2, 26.8, 26.0, 24.8, 24.2, 22.6, 22.4, 18.2, 17.5, 16.0, 15.5, 15.3, 14.1. HR-ESI-MS *m/z* for $C_{38}H_{67}O_5$ $[M+H]^+$: calcd., 603.4910; found: 603.4933.

3.2. Biology

3.2.1. In vitro ACE inhibition assay

The colorimetric method, monitoring the content of hippuric acid (HA) released from the hydrolysis of the substrate hippuryl-histidyl-leucine (HHL), was used to assay the ACE inhibitory activity [82–84]. The test drugs or standard drug was dissolved in the 50 mM sodium borate buffer (pH 8.2, containing 300 mM NaCl). Test or standard drug was pre-incubated with 10 μL of ACE (Sigma-Aldrich, MO, USA) for 10 min at 37 ℃. Then the reaction was initiated by adding 50 μL of the 5 mM HHL (Sigma-Aldrich, MO, USA) and maintained at 37 ℃ for another 0.5 h. 75 μL of 1 M HCl was added to terminate the reaction. After stopping the reaction, 150 μL of pyridine (SD Fine chemical, India) was added followed by 75 μL of Benzene sulfonyl chloride (BSC) (SD Fine chemical, India) (order of addition of reagents is critical) and mixed by inversion for 1 min and cooled on ice. The yellow color developed was determined at 410 nm. The decreased concentration of HA in the test reaction compared with the control reaction was expressed as percentage inhibition and calculated from the equation: ACE inhibition (%) = 100 - $[A_{Test}/A_{Control}] \times 100$, where A_{Test} is the absorbance of sample (test drug, ACE and substrate were present), $A_{Control}$ is the absorbance of control (ACE and substrate were present, 50 mM sodium borate buffer, pH 8.2, containing 300 mM NaCl was used instead of compounds).

The IC_{50} value, defined as the concentration of the inhibitor required to decrease the ACE activity by 50 %, was calculated by non-linear regression according to a plot of percentage ACE inhibition *versus* sample concentrations [85–88].

3.2.2. In vitro cytotoxicity assay

3.2.2.1. Cell culture and treatment. The rat cardiomyoblast H9c2 cell line, purchased from Chinese Academy of Sciences (Shanghai, China), was cultured in Dulbecco's modified Eagle's medium (DMEM; Thermo Fisher Scientific, Beijing, China) supplemented with 10 % fetal bovine serum (FBS; Thermo Fisher Scientific, Beijing, China) and antibiotic regimen (100 U/mL of penicillin and 100 mg/ml of streptomycin) at 37 □ in a humidified atmosphere of 5% CO_2. H9c2 cells were treated with compounds **2e** and **3b** (0–100 μM) for 24 h.

3.2.2.2. Cell viability assay. Cell viability was assessed using the cell counting kit-8 (CCK-8; Solarbio Science & Technology Co., Ltd., Beijing, China) according to the manufacturer's instructions. In brief, H9c2 cells were seeded at a density of 5×10^4 cells/well into 96-well plate and cultured in DMEM-F12 growth medium containing 10 % FBS. Cells were then treated with a series of concentrations of compounds for another 24 h. 10 μL CCK-8 reagent was added to each well, and incubated for 2 h at 37 ℃. The absorbance at 450 nm was measured using a microplate reader.

3.2.3. Molecular modeling

The docking study of the chemical compounds at ACE-binding site was carried out using Autodock 4.2.6 and Autodock Tools 1.5.6 [89]. The 3D crystal structure of human ACE (PDB ID: 1O8A for C-domain, 3NXQ for N-domain) was downloaded from the RCSB Protein Data Bank (http://www.rcsb.org/pdb). Before docking analysis, water molecules and the inhibitor lisinopril were removed, however the cofactors zinc and chloride atoms were retained in the ACE model. Chemical compound structures were generated using ChemBio3D Ultra 14.0 software (CambridgeSoft Co., USA) and their energy was minimized with the MM2 tools in the software to prepare mol2 ligand files. The grid center was placed on a spacing of x: 40.79, y: 33.61 and z: 43.48 with a grid spacing of 0.375 [90]. Binding-energy value was use to determine the best-ranked docking pose of the compound with ACE. *In silico* binding affinities and inhibitory constant (*Ki*) was established through docking the ligands structures of active compounds into the binding pockets of C and N-domain of ACE.

3.2.4. Assessment effects of drugs on zebrafish heart failure

3.2.4.1. Breeding of zebrafish. The wild-type AB line zebrafish were purchased from China Zebrafish Resource Center. Just as we reported previously [91], zebrafish were maintained at 28℃ with a 14/10 h light/dark photoperiod. The feeding scheme of zebrafish were performed according to the Zebrafish book [92]. The zebrafish embryos were generated by mating 5–8 months old fish. Embryos were then raised at 28.5 ℃ in egg water containing 0.003 % 1-phenyl-2-thiourea [93]. The animal protocol was approved by the Scientific Investigation Board of Science and Technology.

3.2.4.2. Determination of no observed adverse effect level. The maximum concentration that did not cause any observable adverse effect was defined as the NOAEL. The NOAEL of all the derivatives and pyxinol were determined by analyzing the toxicity and mortality of zebrafish (2 dpf) treating with each test drug (10, 25, 50, 100, and 200 μg/mL) for 4 h.

3.2.4.3. Zebrafish heart failure model development. The heart in zebrafish is fully formed by 48 h post-fertilization (hpf) [38]. So, in the present study, zebrafish at 48 hpf were selected for Verapamil (Sigma-Aldrich, MO, USA) treatment to develop the heart failure model. The concentration and time of Verapamil treatment were 200 μM and 30 min, respectively [94].

3.2.4.4. Assessment effects of drugs on zebrafish heart failure. Aiming at evaluating the effects of the test compounds (all derivatives, pyxinol, and Enalapril) on heart failure model, 3 zebrafish embryos at 2 dpf were firstly distributed into each well of a 96-well plate, and then pretreated

with each compound (0.5, 1, and 10 μg/mL, respectively) for 4 h. Zebrafish only treated with fresh fish water were used as control group, while those treated with 200 μM verapamil for 30 min. were chosen as the heart failure model fish. Visual observation was performed on each group of zebrafish after verapamil treatment, and images were acquired by using an anatomical stereomicroscope (Olympus Japan) without using an anesthetic. Quantitative image analysis was carried on by using image-based morphometric analysis. Six parameters (heart beats, cardiac output, ejection fraction, fractional shortening, enlarged heart, venous congestion) were calculated to evaluate the cardiac functions [3]. Heart beats were counted for 1 min, and the number of heart beats per unit of time was typically expressed as beats per minute (bpm). The measurements of cardiac output, ejection fraction, fractional shortening, venous congestion area and enlarged heart area were performed according to the images from movies [3]. Shortly, the lengths of the long axis (a) and short axis (b) between the myocardial borders of ventricles at diastole and systole were measured and end systolic or diastolic volumes were calculated with the formula $V = 4/3\pi ab^2$. Cardiac output was the product of stroke volume and heartbeats (1 min). The ejection fraction was calculated by formula: (end-diastolic volume - end systolic end systolic)/(end-diastolic volume) × 100 %. Fractional shortening (%) was calculated using the formula: (length at diastole − length at systole)/(length at diastole) × 100 %.

3.2.5. Metabolomics study

3.2.5.1. Sample collection and extraction. We applied **2e** (1 μg/mL) to 2 dpf zebrafish embryos for metabolite assay. The group were set as: control group zebrafish were treated only with fresh fish water, model group were treated with heart failure-inducing drug verapamil and **2e** group were treated with verapamil and **2e**. And the procedure is consistent with the evaluation method of heart failure efficacy. After 4 h treatment, 10 zebrafish embryos per replicate ($n = 6$) were transferred into 1.5 ml Eppendorf tube and then washed the embryos three time with deionized water. The samples were frozen instantaneously in liquid nitrogen to quench metabolic activity, and stored at −80 °C until further analysis [95].

Zebrafish embryos was thawed in a water bath at room temperature. 250 μL of deionized water was added and homogenized using a high-speed homogenizer. After sonicating 10 s, the homogenate was cooled for 10 s in an ice-water bath, sonicated again 10 s and repeat the operation for 5 min. Subsequently, the sample was freeze-dried, extracted with 80 % methanol. After vortexed about 30 min, the mixture was undergoing centrifugation at 4 °C for 10 min at 10,000 rpm. The supernatant was transferred to a new Eppendorf tube and freeze-dried. The extract was dissolved into 100 μl of 80 % methanol. Prior to injection, the extract were filtered using a syringe filter (0.22 μm). At the same time, 20 μL aliquot of supernatant from each sample was collected and pooled as a quality control (QC) sample for the method validation.

3.2.5.2. UPLC/QTOF-MS. LC–MS analysis was done on a UPLC system equipped with Xevo G2-XS QTOF mass spectrometer (Waters Co., Milford, USA). Separation of the metabolites was conducted on an ACQUITY C18 column (100 mm × 2.1 mm,1.7 μm, Waters Co., Milford, USA) at 40 °C with a flow rate of 0.4 mL/min. Water + 0.1 % formic acid and acetonitrile + 0.1 % formic acid were set as mobile phases A and B, respectively. The elution condition was used: 0−2 min, A: 90 %; 2−26 min, A: 90−0%; 26−28 min, A: 0%; 28–28.1 min, A: 0–90 %; and 28.1−30 min, A: 90 %. 90 % and 10 % acetonitrile aqueous solutions were used as the strong wash solvent and the weak wash solvent, respectively. In present study, the system was equipped with an electrospray ionization (ESI) interface. The main optimized parameters of MS spectrometer were as follows: capillary voltages and cone voltage were 2.2 kV (ESI-) & 2.6 kV (ESI+) and 40 V, respectively; temperatures of source and desolvation were 180 °C and 400 °C, respectively; gas flow rates of cone and desolvation were maintained at 50 l/h and 800 L/h, respectively. In MSE mode, the samples were run at 6 V followed by a collision energy range of 20 V∼40 V to get low and high fragmentation data. Sodium formate was used as calibration from 100 Da to 1000 Da for mass spectrometer. Leucine enkephalin (LE) was used as the external reference and injected with a flow rate of 10 μL/min in ESI+ (m/z 556.2771) and ESI- (m/z 554.2615) modes to ensure accuracy during analysis. Data collecting was conducted on a workstation of MassLynx V4.1 in continuous mode.

3.2.5.3. Metabonomics analysis. —The LCMS data were aligned, deconvoluted and reducted using MarkerLynx XS software (V4.1, Waters, Manchester, UK) [96,97]. The major parameters were set as: the range of mass was $m/z = 100-1000$ Da, both mass window and tolerance were all 0.10, the range of retention time was 0−30 min, the window of retention time was 0.20, minimum intensity was 5%, the threshold of marker intensity was set 500 counts, and the level of noise elimination was 6. In Extended Statistics (XS) Viewer, the RT-m/z pairs with relevant intensities of all detected peaks were listed. The multivariate statistical analysis were performed on SIMCA software (version 15.0, Umetrics, Sweden) to obtain principal component analysis (PCA) and orthogonal projection to latent structures discriminant analysis (OPLS-DA). Furthermore, in order to uncover the potential biomarkers, which were responsible for the difference between model group and **2e** group, VIP (variable importance in the projection)-plots and S-plots were obtained from OPLS-DA. The metabolites with VIP > 1.0 and $p < 0.05$ could be selected as the candidate biomarkers. Moreover, the permutation test was conducted, and the R2/Q2-values indicating the statistical significance were acquired.

Afterwards, some biochemical databases such as HMDB (http://www.hmdb.ca/) and METLIN (http://metlin.scripps.edu/) were used to identify the metabolites. And further confirmation was obtained by comparing with chemical standards or the MS/MS fragmentation patterns. The adducts included [M + Na]+, [M+H]+, [M−H]- and [M + FA-H]-. And the mass tolerance was set at 10 ppm. Next, the MetaboAnalyst 4.0 (http://www.metaboanalyst.ca/) was applied to confirm the special metabolites and to filter out the most important potential metabolic pathways, which impact value was greater than 0.10. Cytoscape was finally used to visualize the metabolic network.

3.2.6. Statistical analysis

One-way ANOVA, followed by Dunnett's test, was used in SPSS 16.0 software (SPSS, USA) to compare the differences between groups, and $p < 0.05$ was considered statistically significant. All data are expressed as mean ± S.D. for quantitative analysis, and results were statistically compared between vehicle-treated and drug-treated zebrafish groups. All experiments were repeated at least three times.

4. Conclusions

This study designed and synthesized 32 fatty acid esterification derivatives of pyxinol for the first time. Among these derivatives, compounds **2e** (IC_{50} = 105 nM) and **3b** (IC_{50} = 114 nM), showed high efficiency on ACE. The molecular docking also showed that **2e** and **3b** exhibited strong hydrogen bonds with key amino acid residues in ACE active sites, with the selectivity towards ACE C-domain inhibition. The *in vivo* assay also demonstrated that **2e** and **3b** markably improved heart beats, venous congestion, heart dilation, cardiac output, ejection fraction and fractional shortening on verapamil-induced zebrafish heart failure model. Moreover, a total of 25 potential biomarkers involving 8 metabolic pathways were identified to further illustrate the anti-HF effect and to understand the preliminary mechanism of **2e** on HF. In conclusion, our data suggested that fatty acid esterified pyxinol derivatives **2e** and **3b** might become novel ACE inhibitor against heart

failure. Further research should be undertaken to investigate the pathways and metabolites.

Funding source

This research was funded by Young and Middle-aged Technology Innovation Leading Talents and Teamsz (Grant No. 20200301002RQ), and the Special Project of Industrial Independent Innovation Ability of Jilin Province (Grant No. 2020C038-3), Supported by Graduate Innovation Fund of Jilin University (Grant No. 101832020CX315).

Declaration of Competing Interest

The authors declare no conflict of interest.

References

[1] M. Metra, J.R. Teerlink, Heart failure, Lancet 390 (2017) 1981–1995.
[2] C.W. Yancy, M. Jessup, B. Bozkutrt, J. Butler, D.E. Casey, M.H. Drazner, G. C. Fonarow, S.A. Geraci, T. Horwich, J.L. Januzzi, M.R. Johnson, E.K. Kasper, W. C. Levy, F.A. Masoudi, P.E. McBride, J.J.V. McMurray, J.E. Mitchell, P.N. Peterson, B. Riegel, F. Sam, L.W. Stevenson, W.H.W. Tang, E.J. Tsai, B.L. Wilkoff, 2013 ACCF/AHA Guideline for the Management of Heart Failure, JACC 62 (2013) 147–239.
[3] F. Tang, X.H. Zhou, L. Wang, L.C. Shan, C.W. Lia, H.F. Zhou, S.M.Y. Lee, M.P. M. Hoi, A novel compound DT-010 protects against doxorubicin-induced cardiotoxicity in zebrafish and H9c2 cells by inhibiting reactive oxygen species-mediated apoptotic and autophagic pathways, Eur. J. Pharmacol. 820 (2018) 86–96.
[4] J. Yang, W.W. Xu, S.J. Hu, Heart Failure: Advanced Development in Genetics and Epigenetics, Biomed Res. Int. 2015 (2015) 1–11.
[5] L.J. Shi, C.P. Mao, Z.C. Xu, L.B. Zhang, Angiotensin-converting enzymes and drug discovery in cardiovascular diseases, Drug Discov. Today 15 (2010) 332–341.
[6] I. Saadaoui, F. Krichen, B.B. Salah, R.B. Mansour, N. Miled, A. Bougatef, M. Kossentini, Design, synthesis and biological evaluation of Schiff bases of 4-amino-1,2,4-triazole derivatives as potent angiotensin converting enzyme inhibitors and antioxidant activities, J. Mol. Struct. 1180 (2019) 344–354.
[7] R. Venkatesh, S. Kasaboina, H.K. Gaikwad, S. Janardhan, R. Bantu, L. Nagarapu, G. N. Sastry, S.K. Banerjee, Design and synthesis of 3-(3-((9H-carbazol-4-yl) oxy)-2-hydroxypropyl)-2-phenylquinazolin-4(3H)-one derivatives to induce ACE inhibitory activity, Eur. J. Med. Chem. 96 (2015) 22–29.
[8] D.J. Newman, G.M. Cragg, Natural Products as Sources of New Drugs from 1981 to 2014, J. Nat. Prod. 79 (2016) 629–661.
[9] I. Yosioka, H. Yamauchi, I. Kitagawa, Lichen Triterpenoids. V.1) On the Neutral Triterpenoids of Pyxine endochrysina NYL, Chem. Pharm. Bull. 20 (1972) 502–513.
[10] F.J. Arriaga, A. Rumbero, E. Wollenweber, Three further dammarane type triterpenes from the frond exudate of the Fern Notholaena rigida, Z. Naturforsch. 51 (1996) 750–752.
[11] N.D. Pokhilo, V.A. Denisenko, V.V. Makhan′kov, N.I. Uvarova, Terpenoids and flavonoids from the leaves of siberian species of the genus Betula, Khim. Prir. Soedin. (1983) 374–375.
[12] U. Kolak, A. Kabouche, M. Ozturk, Z. Kabouche, G. Topçud, A. Ulubelen, Antioxidant diterpenoids from the roots of Salvia barrelieri, Phytochem. Anal. 20 (2009) 320–327.
[13] L. Li, X.Y. Chen, D. Li, D.F. Zhong, Identification of 20(S)-Protopanaxadiol metabolites in human liver microsomes and human hepatocytes, Drug Metab. Dispos. 39 (2011) 472–483.
[14] W.Y. Wang, L. Wang, X.M. Wu, L.X. Xu, Q.G. Meng, W.H. Liu, Stereoselective formation and metabolism of 20(S)-Protopanaxadiol ocotillol type epimers in vivo and in vitro, Chirality 27 (2015) 170–176.
[15] P.Y. Li, J.P. Liu, Y.Y. Ren, C.G. Liu, J.H. Hu, X.J. Du, Preparation Method of 24(R)-ocotillol DQ and Pharmacal Application Thereof, CN102050860A, 2011, 05. 11.
[16] T. Wang, Q. Meng, J. Zhang, Y. Bi, N.C. Jiang, Study on the structure-function relationship of 20(S)-panaxadiol and its epimeric derivatives in myocardial injury induced by isoproterenol, Fitoterapia 81 (2010) 783–787.
[17] P.Y. Li, J.P. Liu, Z. Li, H. Feng, C.Z. Wang, C.G. Liu, Pharmaceutical Uses of Pseudoginsenoside DQ and Derivatives Thereof, CN109700795A, 2019, 05.03.
[18] H.B. Wang, F.H. Fu, Y.T. Jiang, G.Q. Yang, Y.T. Yang, L. Lei, J.B. Ma, R. Zhai, X. L. Qiu, Pharmaceutical Application of Pyxinol, CN106377531A, 2017, 02. 08.
[19] J.J. Chen, T.H. Yang, T.Z. Li, C.A. Geng, X.M. Chen, (20S, 24R)-20, 24-epoxy dammarane-3 Beta, 13 Beta, 25-triol and Application Thereof, CN107778340A, 2018, 03. 09.
[20] J.H. Wang, S.F. Lu, Z.R. Yang, Application of Protopanaxadiol Derivative and Protopanaxatriol Derivative in Preparation of Drugs, CN103961358A, 2014, 08. 06.
[21] G.P.P. Kamatou, R.L.V. Zyl, H. Davids, F.R.V. Heerden, A.C.U. Lourens, A. M. Viljoen, Antimalarial and anticancer activities of selected South African Salvia species and isolated compounds from S. radula, S, S. Afr. J. Bot. 74 (2008) 238–243.
[22] L.N. Atopkina, G.V. Malinovskaya, G.B. Elyakov, N.I. Uvarova, H.J. Woerdenbag, A. Koulman, N. Pras, P. Potier, Cytotoxicity of natural ginseng glycosides and semisynthetic analogues, Planta Med. 65 (1999) 30–34.
[23] J.H. Wang, S.F. Lu, C.J. Xu, W.J. Zhang, Q.L. Wang, Z.R. Yang, Use of 20(S)-protopanoxadiol Derivatives and 20(S)-protopanaxatriol Derivatives in Preparation of Antidepressant Medicines, CN103211823A, 2013, 07. 24.
[24] J.Q. Zhang, Q. Zhang, Y.R. Xu, H.X. Li, F.L. Zhao, C.M. Wang, Z. Liu, P. Liu, Y. N. Liu, Q.G. Meng, F. Zhao, Synthesis and in vitro anti-inflammatory activity of C20 epimeric ocotillol-type triterpenes and protopanaxadiol, Planta Med. 85 (2018) 292–301.
[25] Q.W. Ren, G.Q. Yang, M.Q. Guo, J.W. Guo, Y. Li, J. Lu, Q. Yang, H.H. Tang, Y. Li, X. J. Fang, Y.X. Sun, J.G. Qi, J.W. Tian, H.B. Wang, Design, synthesis, and discovery of ocotillol-type amide derivatives as orally available modulators of P-glycoprotein-mediated multidrug resistance, Eur. J. Med. Chem. 161 (2018) 118–130.
[26] J.Y. Xu, Z.S. Chen, H.Y. Zhang, Y.K. Zhang, Z.W. Zhou, G.X. Wei, Preparation Method and Use of (20S, 24R/S)-epoxy-12 Beta, 25-hydroxy-dammarane-3 Beta-amine Derivatives, CN105985399A, 2016, 10. 05.
[27] K.Y. Wang, Z.W. Zhou, H.Y. Zhang, Y.C. Cao, J.Y. Xu, C. Ma, Q.G. Meng, Y. Bi, Design, synthesis and antibacterial evaluation of 3-substituted ocotillol-type derivatives, Molecules 23 (2018) 3320–3334.
[28] B. Yi, X. Yang, T.T. Zhang, Z.Y. Liu, X.C. Zhang, J. Lu, K.G. Cheng, J.Y. Xu, H. B. Wang, G.Y. Lv, P.J. Lewis, Q.G. Meng, C. Ma, Design, synthesis, nitric oxide release and antibacterial evaluation of novel nitrated ocotillol-type derivatives, Eur. J. Med. Chem. 101 (2015) 71–80.
[29] G.Q. Yang, Y.X. Sun, X.J. Fang, M. Gao, C.H. Wang, H.Y. Gao, Pyxinol Esterification Derivatives Having Anti-inflammatory Activity and Preparing Method and Applications Thereof, CN109776647A, 2019, 05. 21.
[30] Y.X. Sun, X.J. Fang, M. Gao, C.H. Wang, H.Y. Gao, W.J. Bi, H.H. Tang, Y.T. Cui, L. M. Zhang, H.Y. Fan, H. Yu, G.Q. Yang, Synthesis and structure−Activity relationship of pyxinol derivatives as novel anti-inflammatory agents, ACS Med. Chem. Lett. 11 (2020) 457–463.
[31] Y. Bi, J. Yang, C. Ma, Z.Y. Liu, T.T. Zhang, X.C. Zhang, J. Lu, Q.G. Meng, Design, synthesis and in vitro NO-releasing activities of ocotillol-type furoxans, Pharmazie 70 (2015) 213–218.
[32] Z. Liu, Y.R. Xu, X.S. An, J.J. Yang, Q.G. Meng, G.G. Hou, Synthesis and crystal structure of ocotillol-type metabolites derived from (20R)-protopanaxadiol, J. Chem. Res. 41 (2017) 216–220.
[33] Y. Bi, C. Ma, Z.W. Zhou, T.T. Zhang, H.Y. Zhang, X.C. Zhang, J. Lu, Q.G. Meng, P. J. Lewis, J.Y. Xu, Synthesis and antibacterial evaluation of novel hydrophilic ocotillol-type triterpenoid derivatives from 20(S)-Proto- panaxadiol, Rec. Nat. Prod. 9 (2015) 356–368.
[34] E.A. Bae, M.J. Han, E.J. Kim, D.H. Kim, Transformation of ginseng saponins to ginsenoside Rh2 by acids and human intestinal Bacteria and biological activities of their transformants, Arch. Pharm. Res. 27 (2004) 61–67.
[35] H. Hasegawa, K.S. Lee, T. Nagaoka, Y. Tezuka, M. Uchiyama, S. Kadota, I. Saiki, Pharmacokinetics of ginsenoside deglycosylated by intestinal Bacteria and its transformation to biologically active fatty acid esters, Biol. Pharm. Bull. 23 (2000) 298–304.
[36] J.D. Hertog, Chemical Genetics: Drug Screens in Zebrafish, Bioscience Rep. 25 (2005) 289–297.
[37] J. Bakkers, Zebrafish as a model to study cardiac development and human cardiac disease, Cardiovasc. Res. 91 (2011) 279–288.
[38] G. Gu, Y. Na, H. Chung, S.H. Seok, H.Y. Lee, Zebrafish larvae model of dilated cardiomyopathy induced by terfenadine, Korean Circ. J. 47 (2017) 960–969.
[39] N. Mandrekar, N.L. Thakur, Significance of the zebrafish model in the discovery of bioactive molecules from nature, Biotechnol. Lett. 31 (2009) 171–179.
[40] J. Fu, Y.X.R. Tan, Z. Gong, S. Bae, The toxic effect of triclosan and methyl-triclosan on biological pathways revealed by metabolomics and gene expression in zebrafish embryos, Ecotoxicol. Environ. Saf. 189 (2020), 110039.
[41] E. Ortiz-Villanueva, L. Navarro-Martin, J. Jaumot, F. Benavente, V. Sanz-Nebot, B. Pina, R. Tauler, Metabolic disruption of zebrafish (Danio rerio) embryos by bisphenol A. An integrated metabolomic and transcriptomic approach, Environ. Pollut. 231 (2017) 22–36.
[42] S.Y. Wu, N.N. Phan, S.H. Ho, Y.H. Lai, C.H. Tsai, C.H. Yang, H.G. Yu, J.C. Wang, P. L. Huang, Y.C. Lin, Metabolomic assessment of arsenite toxicity and novel biomarker discovery in early development of zebrafish embryos, Toxicol. Lett. 290 (2018) 116–122.
[43] J.N. Hu, J.H. Lee, X.M. Zhu, J.A. Shin, P. Adhikari, J.K. Kim, K.T. Lee, Optimization of lipase-catalyzed synthesis of ginsenoside Rb1 esters using response surface methodology, J. Agr. Food. Chem. 56 (2008) 10988–10993.
[44] N. Li, Y. Huang, W. Xiao, J. Liu, X. Li, P. Li, Synthesis and cytotoxic activities of new fatty acid esters of 20(S)-protopanaxadiol, Ztschrift Für Naturforschung C 66 (2011) 199–204.
[45] Z. Wang, M. Ding, Z. Lin, C. He, Y. Zhao, Esterified derivatives of panaxadiol and their inhibitory effect on HL-60, THP-1, and PC-3 cell lines, Chem. Biodivers. 16 (2019), e1900188.
[46] G.Q. Wei, Y.N. Zheng, W. Li, W.C. Liu, T. Lin, W.Y. Zhang, H.F. Chen, J.Z. Zeng, X. K. Zhang, Q.C. Chen, Structural modification of ginsenoside Rh(2) by fatty acid esterification and its detoxification property in antitumor, Bioorg. Med. Chem. Lett. 22 (2012) 1082–1085.
[47] P. Wang, X.L. Bi, Y.M. Guo, J.Q. Cao, S.J. Zhang, H.N. Yuan, H.R. Piao, Y.Q. Zhao, Semi-synthesis and anti-tumor evaluation of novel 25-hydroxyprotopanaxadiol derivatives, Eur. J. Med. Chem. 55 (2012) 137–145.

[48] X.J. Li, Z.C. Du, Y. Huang, B.M. Liu, W.J. Hu, W.J. Lu, J.G. Deng, Synthesis and hypoglycemic activity of esterified-derivatives of mangiferin, Chin. J. Nat. Med. 11 (2013) 296–301.
[49] H. Hasegawa, Proof of the mysterious efficacy of ginseng: basic and clinical trials: metabolic activation of ginsenoside: deglycosylation by intestinal Bacteria and esterification with fatty acid, J. Pharmacol. Sci. 95 (2004) 153–157.
[50] O. Abdelhedi, R. Nasria, L. Morab, M. Jridia, F. Toldráb, M. Nasri, In silico analysis and molecular docking study of angiotensin I-converting enzyme inhibitory peptides from smooth-hound viscera protein hydrolysates fractionated by ultrafiltration, Food Chem. 239 (2018) 453.
[51] D. Addla, A. Jallapally, A. Kanwal, B. Sridhar, S.K. Banerjee, S. Kantevari, Design, synthesis and evaluation of novel 2-hydroxypyrrolobenzodiazepine -5,11-dione analogues as potent angiotensin converting enzyme (ACE) inhibitors, Bioorg. Med. Chem. Lett. 21 (2013) 4485–4493.
[52] A.T. Nchinda, K. Chibale, P. Redelinghuysa, E.D. Sturrock, Synthesis and molecular modeling of a lisinopril-tryptophan analogue inhibitor of angiotensin I-converting enzyme, Bioorgan. Med. Chem. Lett. 16 (2006) 4616–4619.
[53] T. Zhang, S.P. Nie, B.Q. Liu, Y.D. Yu, Y. Zhang, J.B. Liu, Activity prediction and molecular mechanism of bovine blood derived angiotensin I-Converting enzyme inhibitory peptides, PLoS One 10 (2015), e0119598.
[54] H.R. Corradi, I. Chitapi, B.T. Sewell, D. Georgiadis, V. Dive, E.D. Sturrock, K. R. Acharya, The structure of testis angiotensin-converting enzyme in complex with the C domain-specific inhibitor RXPA380, Biochemistry 46 (2007) 5473–5478.
[55] V.K. Jimsheena, L.R. Gowda, Colorimetric, High-Throughput Assay for Screening Angiotensin I-Converting Enzyme Inhibitors, Anal. Chem. 81 (2009) 9388–9394.
[56] V.K. Jimsheena, L.R. Gowda, Angiotensin I-converting enzyme (ACE) inhibitory peptides derived from arachin by simulated gastric digestion, Food Chem. 125 (2011) 561–569.
[57] K. Kucukoglu, F. Oral, T. Aydin, C. Yamali, O. Algul, H. Sakagami, I. Gulcin, C. T. Supuran, H.I. Gul, Synthesis, cytotoxicity and carbonic anhydrase inhibitory activities of new pyrazolines, J. Enzyme Inhib. Med. Chem. 31 (2016) 20–24.
[58] T. Dastan, U.M. Kocyigit, S. Durna Dastan, P. Canturk Kilickaya, P. Taslimi, O. Cevik, M. Koparir, C. Orek, I. Gulcin, A. Cetin, Investigation of acetylcholinesterase and mammalian DNA topoisomerases, carbonic anhydrase inhibition profiles, and cytotoxic activity of novel bis(alpha-aminoalkyl)phosphinic acid derivatives against human breast cancer, J. Biochem. Mol. Toxicol. 31 (2017), e21971.
[59] M. Tugrak, H. Inci Gul, H. Sakagami, I. Gulcin, C.T. Supuran, New azafluorenones with cytotoxic and carbonic anhydrase inhibitory properties: 2-Aryl-4-(4-hydroxy-phenyl)-5H-indeno[1,2-b]pyridin-5-ones, Bioorg. Chem. 81 (2018) 433–439.
[60] D. Ozmen Ozgun, H.I. Gul, C. Yamali, H. Sakagami, I. Gulcin, M. Sukuroglu, C. T. Supuran, Synthesis and bioactivities of pyrazoline benzensulfonamides as carbonic anhydrase and acetylcholinesterase inhibitors with low cytotoxicity, Bioorg. Chem. 84 (2019) 511–517.
[61] S. Ouchi, T. Miyazaki, K. Shimada, Y. Sugita, M. Shimizu, A. Murata, T. Kato, T. Aikawa, S. Suda, T. Shiozawa, M. Hiki, S. Takahashi, H. Iwata, T. Kasai, K. Miyauchi, H. Daida, Low docosahexaenoic acid, dihomo-gamma-Linolenic acid, and arachidonic acid levels associated with long-term mortality in patients with acute decompensated heart failure in different nutritional statuses, Nutrients 9 (2017).
[62] J. Xu, X.Y. Li, F.B. Zhang, L.Y. Tang, J.Y. Wei, X.Q. Lei, H.H. Wang, Y. Zhang, D. F. Li, X. Tang, G. Li, S.H. Tang, H.W. Wu, H.J. Yang, Integrated UPLC-Q/TOF-MS technique and MALDI-MS to study of the efficacy of YiXinshu capsules against heart failure in a rat model, Front. Pharmacol. 10 (2019) 1474.
[63] Y. Wang, C. Li, Z.Y. Liu, T.J. Shi, Q.Y. Wang, D. Li, Y. Wu, J. Han, S.Z. Guo, B. H. Tang, W. Wang, Dan Qi, Pill protects against heart failure through the arachidonic acid metabolism pathway by attenuating different cyclooxygenases and leukotrienes B4, BMC Complement. Altern. Med. 14 (2014) 67–77.
[64] M. Harada, N. Takeda, H. Toko, Prostaglandin E2 signaling as a target of anti-cardiac fibrosis in heart failure treatment, Int. Heart J. 58 (2017) 3–4.
[65] X.S. Gu, J. Xu, L.P. Zhu, T. Bryson, X.P. Yang, E. Peterson, P. Harding, Prostaglandin E2 reduces cardiac contractility via EP3 receptor, Circ. Heart Fail. 9 (2016).
[66] V.S. Hanna, E.A.A. Hafez, Synopsis of arachidonic acid metabolism: a review, J. Adv. Res. 11 (2018) 23–32.
[67] C. Li, J. Wang, Q.Y. Wang, Y. Zhang, N. Zhang, L.H. Lu, Y. Wu, Q. Zhang, W. Wang, Y. Wang, P.F. Tu, Qishen granules inhibit myocardial inflammation injury through regulating arachidonic acid metabolism, Sci. Rep. 6 (2016) 36949.
[68] X. Wang, Y.H. Gao, Y.H. Tian, X. Liu, G.H. Zhang, Q. Wang, W.Y. Xie, K. Liu, Q. Qian, Q. Wang, Integrative serum metabolomics and network analysis on mechanisms exploration of Ling-Gui-Zhu-Gan Decoction on doxorubicin-induced heart failure mice, J. Ethnopharmacol. 250 (2020), 112397.
[69] S. AbdAlla, X.B. Fu, S.S. Elzahwy, K. Klaetschke, T. Streichert, U. Quitterer, Up-regulation of the cardiac lipid metabolism at the onset of heart failure, Cardiac. Lipid Metabolism in Heart Failure 9 (2011) 190–206.
[70] J.P. Huang, M.L. Cheng, C.H. Wang, M.S. Shiao, J.K. Chen, L.M. Hung, High-fructose and high-fat feeding correspondingly lead to the development of lysoPC-associated apoptotic cardiomyopathy and adrenergic signaling-related cardiac hypertrophy, Int. J. Cardiol. 215 (2016) 65–76.
[71] P.M. Finglas, Dietary reference intakes for Thiamin, Riboflavin, niacin, vitamin B6, folate, vitamin B12, pantothenic acid, biotin and choline, Trends in Food Sci. Tech. 11 (2001) 296–298.
[72] B.J. Bennett, T.Q. de Aguiar Vallim, Z.N. Wang, D.M. Shih, Y.H. Meng, J. Gregory, H. Allayee, R. Lee, M. Graham, R. Crooke, P.A. Edwards, S.L. Hazen, A.J. Lusis, Trimethylamine-N-oxide, a metabolite associated with atherosclerosis, exhibits complex genetic and dietary regulation, Cell Metab. 17 (2013) 49–60.
[73] W. Shuai, J.Y. Wen, X.L. Li, D. Wang, Y.D. Li, J. Xiang, High-choline diet exacerbates cardiac dysfunction, fibrosis, and inflammation in a mouse model of heart failure with preserved ejection fraction, J. Card. Fail. 26 (2020) 694–702.
[74] S. Maekawa, S. Takada, H. Nambu, T. Furihata, N. Kakutani, D. Setoyama, Y. Ueyanagi, D. Kang, H. Sabe, S. Kinugawa, Linoleic acid improves assembly of the CII subunit and CIII2/CIV complex of the mitochondrial oxidative phosphorylation system in heart failure, Cell Commun. Signal 17 (2019) 128.
[75] F. Zhang, Q. Zhan, X. Dong, B. Jiang, L.N. Sun, S.H. Gao, Z.Q. He, X. Tao, W. S. Chen, Shengxian decoction in chronic heart failure treatment and synergistic property of Platycodonis Radix: a metabolomic approach and its application, Mol. Biosyst. 10 (2014) 2055–2063.
[76] M. Knapp, M. Baranowski, A. Lisowska, W. Musial, Decreased free sphingoid base concentration in the plasma of patients with chronic systolic heart failure, Adv. Med. Sci. 57 (2012) 100–105.
[77] T.H. Cao, D.J.L. Jones, A.A. Voors, P.A. Quinn, J.K. Sandhu, D.C.S. Chan, H. M. Parry, M. Mohan, I.R. Mordi, I.E. Sama, S.D. Anker, J.G. Cleland, K. Dickstein, G. Filippatos, H.L. Hillege, M. Metra, P. Ponikowski, N.J. Samani, D.J. Van Veldhuisen, F. Zannad, C.C. Lang, L.L. Ng, Plasma proteomic approach in patients with heart failure: insights into pathogenesis of disease progression and potential novel treatment targets, Eur. J. Heart Fail. 22 (2020) 70–80.
[78] L.R. Gray, S.C. Tompkins, E.B. Taylor, Regulation of pyruvate metabolism and human disease, Cell. Mol. Life Sci. 71 (2014) 2577–2604.
[79] C.H. Wang, M.L. Cheng, M.H. Liu, Simplified plasma essential amino acid-based profiling provides metabolic information and prognostic value additive to traditional risk factors in heart failure, Amino Acids 50 (12) (2018) 1739–1748.
[80] M.C. Liu, Y.X. Li, Y.Q. Tang, L. Zheng, C. Peng, Synergistic effect of Aconiti Lateralis Radix praeparata water-soluble alkaloids and Ginseng Radix et Rhizoma total ginsenosides compatibility on acute heart failure rats, J. Chromatogr. B Analyt. Technol. Biomed. Life Sci. 1137 (2020), 121935.
[81] A. Rafighdoost, F. Vakilian, A. Rafighdoost, A. Amin, M. Salehi, Liver enzymes and uric acid in acute heart failure, Res. Cardiovasc. Med. 4 (2015).
[82] P.K. Kalavagunta, P.K. Bagul, A. Jallapally, S. Kantevari, S.K. Banerjee, N. Ravirala, Design and green synthesis of 2-(diarylalkyl)aminobenzothiazole derivatives and their dual activities as angiotensin converting enzyme inhibitors and calcium channel blockers, Eur. J. Med. Chem. 83 (2014) 344–354.
[83] S.M. Auwal1, N.Z. Abidin, M. Zarei, C.P. Tan, N. Saari, Identification, structure-activity relationship and in silico molecular docking analyses of five novel angiotensin I-converting enzyme (ACE)-inhibitory peptides from stone fish (Actinopyga lecanora) hydrolysates, PLoS One 14 (2019), e0197644.
[84] T. Hai-Bang, K. Shimizu, Structure–activity relationship and inhibition pattern of reishi-derived (Ganoderma lingzhi) triterpenoids against angiotensin-converting enzyme, Phytochem. Lett. 12 (2015) 243–247.
[85] I. Gulcin, B. Trofimov, R. Kaya, P. Taslimi, L. Sobenina, E. Schmidt, O. Petrova, S. Malysheva, N. Gusarova, V. Farzaliyev, A. Sujayev, S. Alwasel, C.T. Supuran, Synthesis of nitrogen, phosphorus, selenium and sulfur-containing heterocyclic compounds-Determination of their carbonic anhydrase, acetylcholinesterase, butyrylcholinesterase and alpha-glycosidase inhibition properties, Bioorg. Chem. 103 (2020), 104171.
[86] E. Bursal, P. Taslimi, A.C. Gören, İ. Gülçin, Assessments of anticholinergic, antidiabetic, antioxidant activities and phenolic content of Stachys annua, Biocatal. Agric. Biotechnol. 28 (2020), 101711.
[87] F. Turkan, Z. Huyut, P. Taslimi, M.T. Huyut, I. Gulcin, Investigation of the effects of cephalosporin antibiotics on glutathione S-transferase activity in different tissues of rats in vivo conditions in order to drug development research, Drug Chem. Toxicol. 43 (2020) 423–428.
[88] C. Caglayan, P. Taslimi, C. Turk, I. Gulcin, F.M. Kandemir, Y. Demir, S. Beydemir, Inhibition effects of some pesticides and heavy metals on carbonic anhydrase enzyme activity purified from horse mackerel (Trachurus trachurus) gill tissues, Environ. Sci. Pollut. Res. Int. 27 (2020) 10607–10616.
[89] G.M. Morris, R. Huey, W. LindstromI, M.F. Sanner, R.K. Belew, D.S. Goodsell, A. J. Olson, Software news and updates AutoDock4 and AutoDockTools4: automated docking with selective receptor flexibility, J. Comput. Chem. 30 (2009) 2785–2791.
[90] X.M. Wang, H.X. Chen, X.G. Fu, S.Q. Li, J. Wei, A novel antioxidant and ACE inhibitory peptide from rice bran protein: biochemical characterization and molecular docking study, LWT - Food Sci. Technol. 75 (2017) 93–99.
[91] Y.W. Gou, W. Sun, L.L. Liu, M.M. Zhang, J.N. Du, R.N. Wang, X.S. Xu, Construction of irf4a transgenic zebrafish using Tol2 system and its potential application, DoseResponse 22 (2020) 1–9.
[92] M. Westerfield M, The Zebrafish Book: A Guide for the Laboratory Use of Zebrafish (Danio rerio), University Of Oregon Press, EugeneOR, 1995.
[93] H.L. Quan, G.C. Oh, S.H. Seok, H.Y. Lee, Fimasartan, an angiotensin II receptor antagonist, ameliorates an in vivo zebrafsh model of heart failure, Korean J. Intern. Med. (2020).
[94] X.Y. Zhu, S.Q. Wu, S.Y. Guo, H. Yang, B. Xia, P. Li, C.Q. Li, A zebrafish heart failure model for assessing therapeutic agents, Zebrafish 15 (2018) 243–253.
[95] X.Q. Ren, H.J. Zhang, N.B. Geng, L.G. Xing, Y. Zhao, F.D. Wang, J.P. Chen, Developmental and metabolic responses of zebrafish (Danio rerio) embryos and larvae to short-chain chlorinated paraffins (SCCPs) exposure, Sci. Total Environ. 622-623 (2018) 214–221.
[96] Y.R. Wang, C.Z. Wang, H.Q. Lin, Y.H. Liu, Y.M. Li, Y. Zhao, P.Y. Li, J.P. Liu, Discovery of the potential biomarkers for discrimination between Hedyotis diffusa and Hedyotis corymbosa by UPLC-QTOF/MS metabolome analysis, Molecules 23 (2018) 1525.
[97] C.Z. Wang, Y.Z. Yuan, H. Pan, A.C. Hsu, J.L. Chen, J.P. Liu, P.Y. Li, F. Wang, Protective effect of Ocotillol, the derivate of Ocotillol-Type Saponins in Panax

genus, against acetic acid-induced gastric ulcer in rats based on untargeted metabolomics, Int. J. Mol. Sci. 21 (2020) 2577.